General Disclaimer

One or more of the Following Statements may affect this Document

- This document has been reproduced from the best copy furnished by the organizational source. It is being released in the interest of making available as much information as possible.

- This document may contain data, which exceeds the sheet parameters. It was furnished in this condition by the organizational source and is the best copy available.

- This document may contain tone-on-tone or color graphs, charts and/or pictures, which have been reproduced in black and white.

- This document is paginated as submitted by the original source.

- Portions of this document are not fully legible due to the historical nature of some of the material. However, it is the best reproduction available from the original submission.

OPTIMUM SATELLITE ORBITS FOR ACCURATE MEASUREMENT OF THE EARTH'S RADIATION BUDGET, SUMMARY

(CSU-ATSP-289-US-ISSN-0067-0340) OPTIMUM SATELLITE ORBITS FOR ACCURATE MEASUREMENT OF THE EARTH'S RADIATION BUDGET, SUMMARY Final Report (Colorado State Univ.) 65 p
HC A04/MF A01

N79-10076

CSCL 22A G3/13

Unclas
15304

by

G. G. CAMPBELL and T. H. VONDER HAAR

Atmospheric Science
PAPER NO.
289

US ISSN 0067-0340

DEPARTMENT OF ATMOSPHERIC SCIENCE
COLORADO STATE UNIVERSITY
FORT COLLINS, COLORADO

OPTIMUM SATELLITE ORBITS FOR ACCURATE MEASUREMENT OF THE EARTH'S RADIATION BUDGET, SUMMARY

by

G.G. Campbell and T.H. Vonder Haar

FINAL REPORT

NASA CONTRACT NAS 1-13106

NATIONAL AERONAUTICS AND SPACE ADMINISTRATION
LANGLEY RESEARCH CENTER

FROM

DEPARTMENT OF ATMOSPHERIC SCIENCE
COLORADO STATE UNIVERSITY
THOMAS H. VONDER HAAR, PRINCIPAL INVESTIGATOR

Atmospheric Science Paper No. 239

APRIL 1978

TABLE OF CONTENTS

ABSTRACT

The optimum set of orbit inclinations for the measurement of the earth radiation budget from spacially integrating sensor systems has been estimated for two and three satellite systems. The best set of the two were satellites at orbit inclinations of 80^{o} and 50^{o}; of three the inclinations were 80^{o}, 60^{o} and 50^{o}. These were chosen on the basis of a simulation of flat plate and spherical detectors flying over a daily varying earth radiation field as measured by the Nimbus III medium resolution scanners. A diurnal oscilation was also included in the emitted flux and albedo to give a source field as realistic as possible. Twenty-three satellites with different inclinations and equator crossings were simulated allowing the results of thousand of multi-satellite sets to be intercompared. All were circular orbits of radius 7178 kilometers.

The analysis scheme is critical to the measurement of the radiation budget, so several are discussed. The most important part of the analysis is to compensate for the diurnal variation in the radiation field with the limited local time sampling of a few satellites. Also, the flux measured at satellite altitude is a smoothed version of the top of the atmosphere flux, so the deconvolution is discussed to remove some of this smoothing.

The internal error (reproducibility) of many orbit inclination systems is listed, as well as their error relative to a perfect measurement system (accuracy). The error of the 80, 50 system is $\pm$ 3.3 w/m^2 and for 80, 60, 50 is $\pm$ 2.4 w/m^2 for latitude zonal averages of emitted flux. The largest source of error was imperfect local time sampling. The deconvolution scheme was found to improve the resolution of the emitted flux, but not the reflected flux because of the amplication of noise.

I. INTRODUCTION

There is a very large demand for various forms of radiation measurements of the earth, ocean-atmosphere system on a global scale (Science Applications for Satellite Radiation Measurements, 1975; Earth Radiation Budget Science Workshop, 1978). Essentially, there are two main divisions in the desired measurements. One of these measurements, taken all over the globe, for a limited time period to develop radiation parameterization schemes for atmospheric modeling. The other is a long term, large scale, monitoring of the earth for climate studies.

The Earth Radiation Budget Experiment has addressed this second problem and has designed satellites to make the measurement. The measurements will monitor the present radiation climate on a space scale of 10^6 km^2 and a time resolution of about a month. This can be used to develop empirical climate models by comparison of surface activity to the radiation budget. It will also verify other theoretical climate models. Ultimately, it may provide the raw data for forecasting climate and climate changes.

This particular study assesses the accuracy of different satellite systems and seeks the best orbital configuration for making the measurement. Integrating sensors like flat plates or spheres have been proposed because of their simplicity and stability. Individual measurements of a particular location in space and time are simulated numerically over realistic radiation fields. The location of measurements produced by several satellites in a month are combined to generate monthly average measurements at satellite altitude. Thousands of different orbit inclination combinations have been intercompared. In addition, a reference measurement has been made with uniform space and time sampling (e.g. a sky full of satellites) to minimize the effects of different analysis

schemes in the comparisons. In conclusion, accuracies of the best systems found are discussed.

In the final section, a discussion is made of deconvolution techniques to predict the radiation fluxes at the top of the atmosphere rather than at satellite altitude. This provides more specificity for the climate modeling problem but it may not be as accurate.

II. SINGLE POINT MEASUREMENTS; THE SIMULATION MODEL

A single measurement is the integral of the radiation flux from each differential segment of the field of view. No mixing of the two channels, reflected and emitted, is considered nor are degradation or calibration, electronic noise etc. considered as these are handled by others on the E^3 team. The measurement of course depends on the geometry of the sensor and its altitude. Daily average surface characteristics come from real measurements made by scanner on Nimbus III (Raschke et al., 1973). Limb darkening effects, bidirectional reflectance and diurnal variations are also included. The integral is then simulated by breaking up the field of view into more than 50 different segments.

The model is reasonably realistic but more important it is as complicated as the real world (Fig. 1). The fundamental assumption is that the relative accuracy of averages of individual numerical results correspond to the relative accuracy of real measurements over the real world.

The Nimbus III real data set (Raschke et al., 1973), Figs. 2 and 3, overcomes the need to fake day to day changes of atmospheric conditions. The data were taken by a scanner at noon and midnight with a $10^5 km^2$ resolution. The infrared data used in simulation is the average power emitted from the top of the

PROGRAM GENDAT

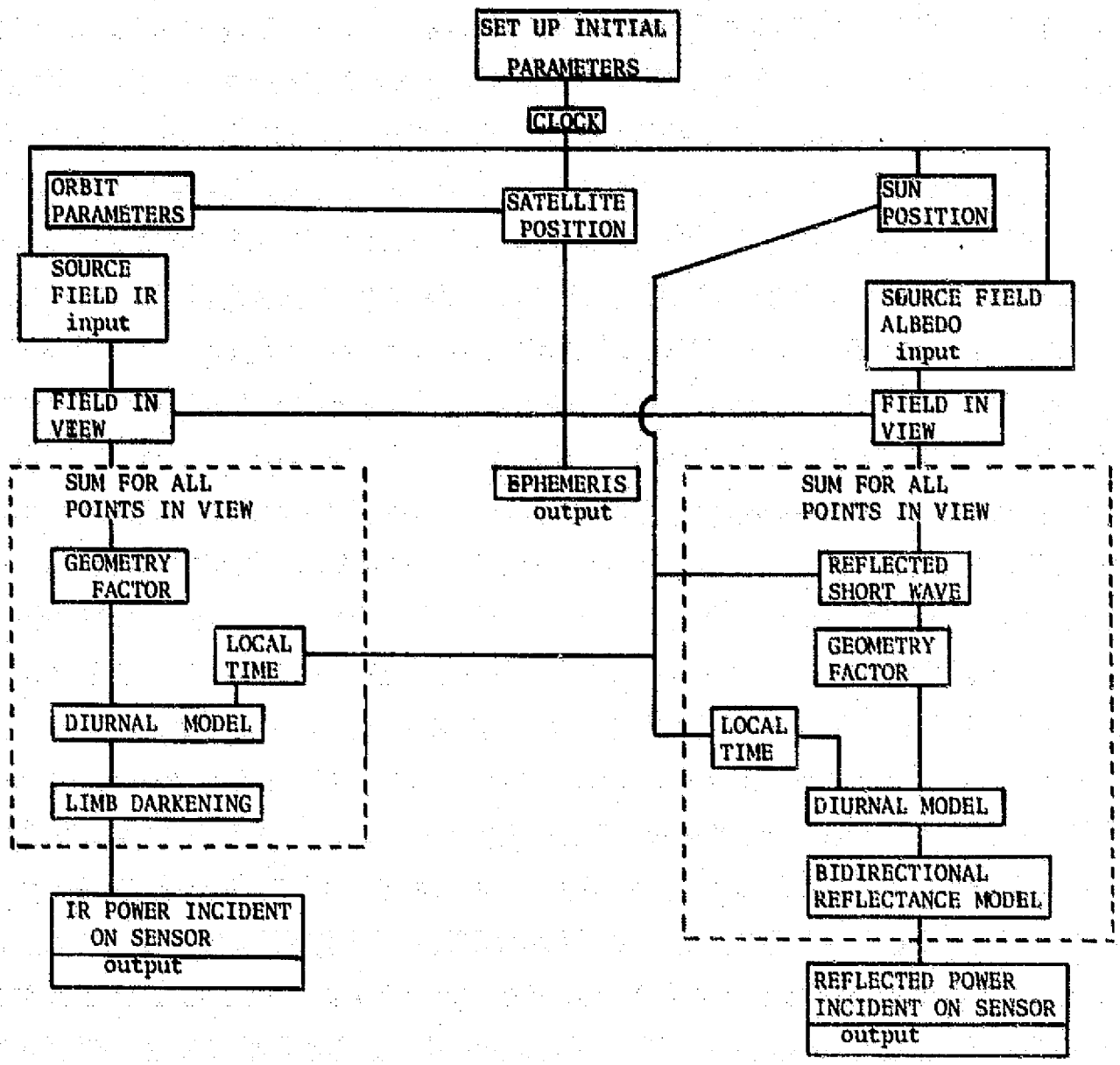

Figure 1

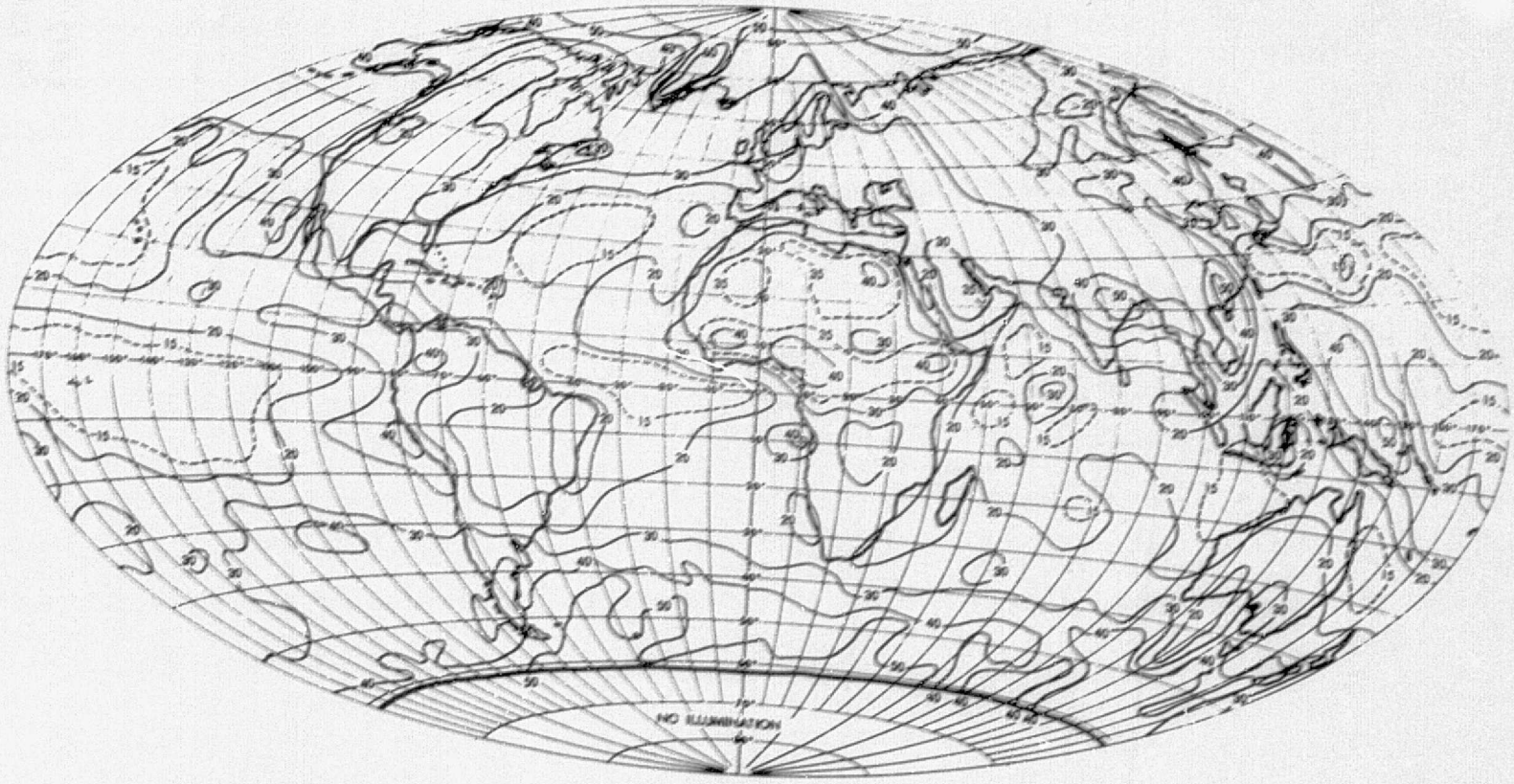

Figure 2. Albedo (percent) of the Earth-atmosphere system during the period July 16-31, 1969.

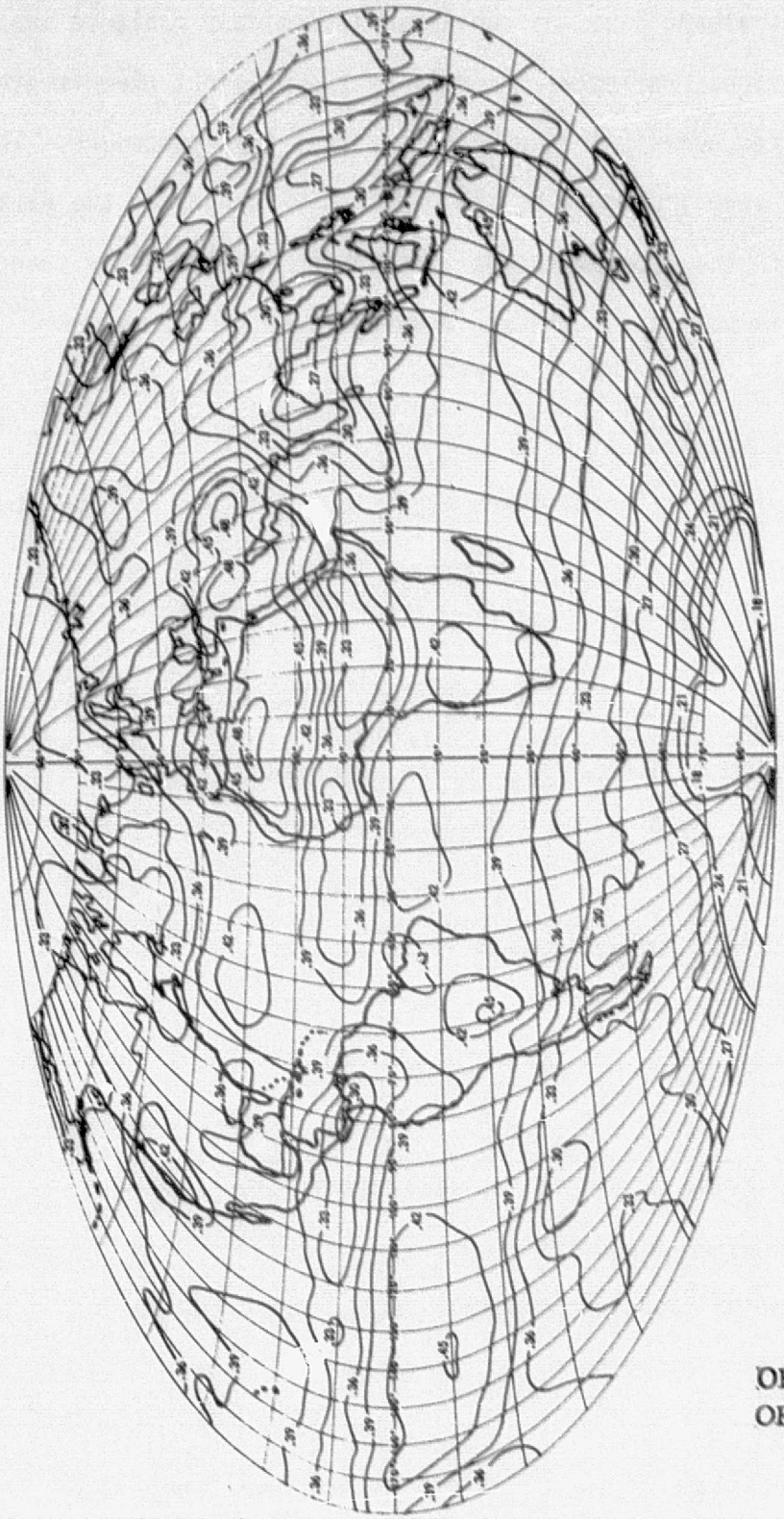

Figure 3. Emitted flux (cal/cm^2 min) from the Earth-atmosphere system during the period July 16-21, 1969.

atmosphere, a linear average of the midday and midnight measurements. The daily average albedo data was converted from midday radiance measurements with bidirectional reflectance models by the original experimenters. Essentially the numerical simulation reverses this procedure. The use of this data is very important as the day to day changes on the earth are realistic. In the program the data is in the form of daily changing maps with 6644 grid points for the whole earth.

A. Emitted Component

An individual infrared measurement is represented in Equation 1.

$$m(\theta_s^{\phi},\phi_s)^{\phi} = 4\pi \int s_{IR}\,(\theta,\,\phi)\; c(\hat{r}\cdot\hat{r}_s)\;\frac{\vec{r}\cdot\vec{r}_e}{r^3}\;D(\theta,\,\phi-\phi_{sun})\;\cdot \qquad (1)$$

$$L(\hat{r}\cdot\hat{r}_e)\;\gamma\;(\hat{r}\cdot\hat{r}_e)\;r_e\,d\Omega$$

s_{IR} = emitted power at top of the atmosphere

c = geometry factor = 1 for sphere

= $\hat{r}\cdot\hat{r}_s$ for plate

D = diurnal variation from Tiros IV

L = limb darkening

γ = field of view stop = 1, $\hat{r}\cdot\hat{r}_e > 0$

= 0, $\hat{r}\cdot\hat{r}_e < 0$

$(\theta_s,\,\phi_s)$ = location of satellite, (colatitude, longitude)

$(\theta,\,\phi)$ = location of source

$\vec{r}_s$ = vector location of satellite

$\vec{r}_e$ = vector location of source point

$\vec{r}$ = $\vec{r}_s - \vec{r}_e$

ϕ_{sun} = longitude of sun which determines local time

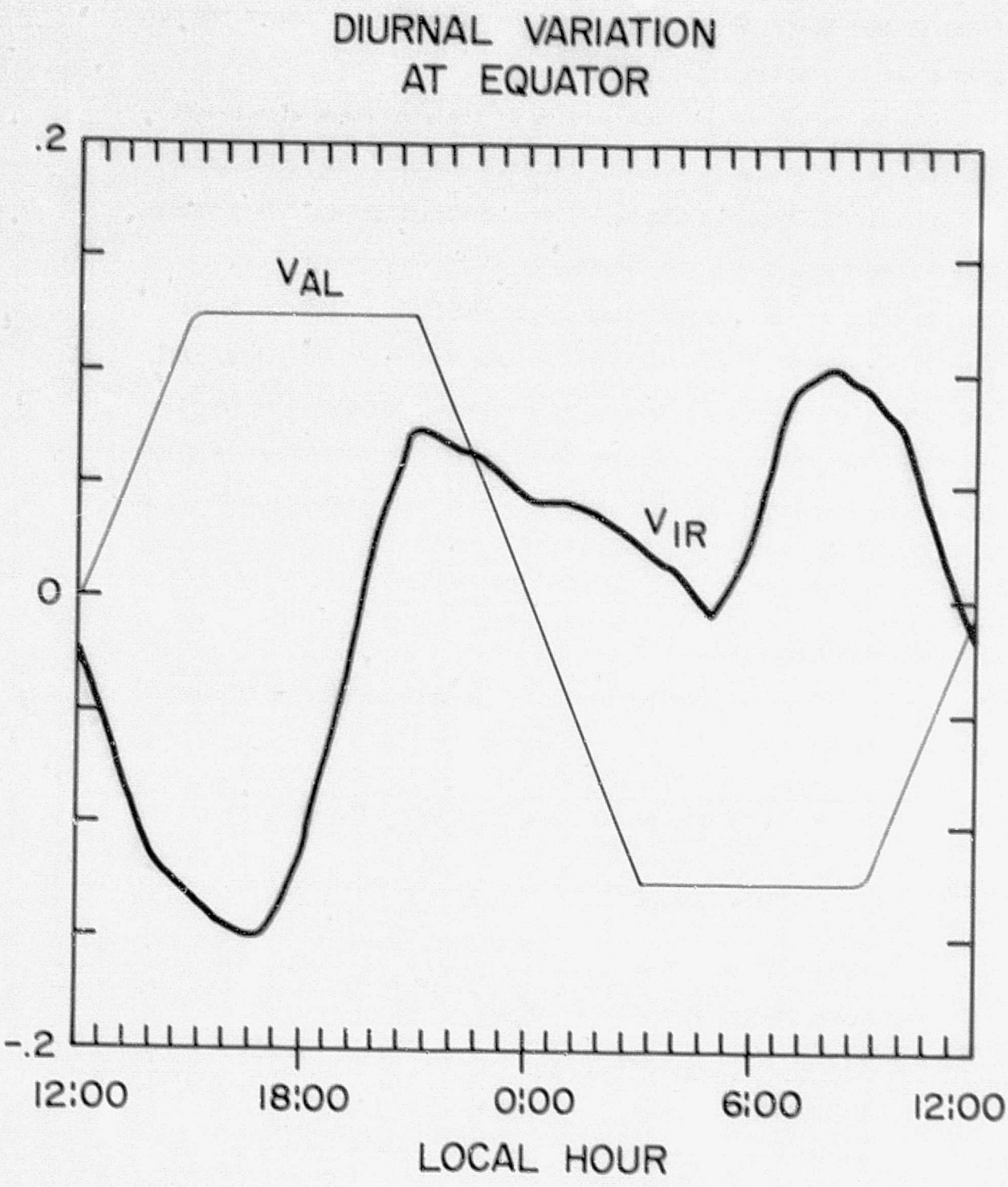

Figure 4

The source, s_{IR}, comes from the Nimbus III maps. The diurnal variation, D (Fig. 4) was estimated from Tiros IV measurements at different local times,(Vonder Haar, 1968). This variation is damped out toward the poles with a sin θ factor.

Limb darkening arises from cooling of the atmosphere with height and its absorbtion and emission of infrared energy. The factor used was extrapolated from the Nimbus III data analysis scheme. This variation is small decreasing the radiance by 4% at large angles.

In order to perform the integration, the field of view is broken into 50 components of approximately the same radiative influence. All the factors are calculated separately for each point depending on its relative location to the observing point. Finer resolution would slightly improve the results. The resolution is a compromise between accuracy and computation time.

B. Reflected Component

The reflected power measurement, n, is more complex as it depends on the sun's location.

$$n(\theta_s, \phi_s) = \int \alpha(\theta, \phi)\, d(\theta, \phi-\phi_{sun})\, \hat{r}_e\cdot\hat{r}_{sun}\, I(\hat{r}_e\cdot\hat{r}_{sun}, t)\cdot \rho(\theta,\phi, \hat{r}_e\cdot\hat{r}_{sun}, \hat{r}_e\cdot\hat{r}, \hat{r}\cdot\hat{r}_{sun})\, \frac{\hat{r}_e\cdot\hat{r}}{r^2}\, g_\gamma\, r_e^2\, d\Omega \qquad (2)$$

α = daily average albedo

d = crude diurnal variation of albedo

I = $I_o\, r^2_{sun}/r^2_{sun,av}$ for $\hat{r}_e\cdot\hat{r}_{sun} > 0$ day

= o night

the time dependence arises from the earth's elliptical orbit

ρ = bidirectional reflectance

$\vec{r}_{sun}$ = earth sun vector

$r_{sun, av}$ = average earth sun distance

The daily average albedo, α is the ratio of the reflected energy flux over the day to the incident flux.

$$\alpha(\theta,\phi) = \frac{\int_0^1 \int_{2\pi}^{0} N(\theta,\phi,\theta_{sun},\phi_{sun},\gamma,\beta) \cos\alpha \, d\cos\gamma \, d\beta \, d\phi_{sun}}{\int_0^{2\pi} I \, d\phi_{sun}} \quad (3)$$

N = reflected radiance

(γ,β) = direction of reflection

The reflected radiance can be calculated from the normalized bi-direction reflectance coefficient which represents the varying reflectivity of the surface.

$$N = \alpha\rho \; I \; \hat{r}_e \cdot \hat{r}_{sun} \quad (4)$$

For purposes of calculation ρ can be separated into an anisotropic factor, χ, and a zenith angle dependent function, F,

$$\rho = \frac{F(\hat{r}_e \cdot \hat{r}_{sun})}{\bar{F}} \frac{}{\pi\chi(\hat{r}_e \cdot \hat{r}_{sun}, \hat{r}_e \cdot \hat{r}, \hat{r} \cdot \hat{r}_{sun}, \theta, \phi)} \quad (5)$$

χ and F are normalized so that if α is one all the incident energy is reflected

$$\int_{2\pi} \frac{1}{\pi\chi} \, d\cos\gamma \, d\beta = 1 \quad (6)$$

and

$$\int_{\text{daylight}} F(\hat{r}_e \cdot \hat{r}_{sun}) \; I \; \hat{r}_e \cdot \hat{r}_{sun} \, d\phi_{sun} = \bar{F} \quad (7)$$

The χ and F were tabulated in the Nimbus III experiment from airplane and surface data for a limited range of zenith angle (less than 60^0), (Sikula and Vonder Haar, 1972). These were extrapolated to predict the radiance at any angle. Only two surface types were used in the model; a land cloud ρ_c

and a ρ_o for the clear ocean. Experiments are now being performed by NASA to obtain these factors more accurately for all angles on many different surface types (ERB, Nimbus-6, 1975).

The diurnal variation in albedo is a crude representation of the variation measured by Tiros IV (Fig. 4).

$$d = [1 + v(\phi - \phi_{sun}) \sin \theta] \tag{8}$$

The v factor is chosen as an antisymmetric function negative before noon and positive after noon. The antisymmetric property is used so that the energy weighted average of v is zero and the average albedo is unchanged (Eq. 9).

$$\begin{aligned} \int \alpha\, d\, I\, \hat{r}_e \cdot \hat{r}_{sun}\, d\phi_{sun} &= \alpha \int (1 + v \sin\theta)\, I\, \hat{r}_e \cdot \hat{r}_{sun}\, d\phi_{sun} \\ &= \alpha \int I\, \hat{r}_e \cdot \hat{r}_{sun}\, d\phi_{sun} \end{aligned} \tag{9}$$

Improvements are possible in d and ρ with future physical measurements. The simple form of d is especially bad for sun synchronous simulation experiments as d for these sensors do not change at a given locale.

Large numbers of measurements can now be made from any place in space and time. The average computer time required is .01 seconds on a CDC 7600 computer per measurement.

III. MEASUREMENT ORBITS; GEOMETRICAL SAMPLING

Simple circular orbits are used to simplify the analysis procedure. The orbit planes precess because of the quadrapole moment of the earth's gravitational field. Individual measurements are spaced along the orbit three to four minutes apart, corresponding to greatly changed fields of view. For this study orbit radii of 7178 km have been used to assure that

real space vehicles will have at least 5 year orbital lifetime. Finally all the simulated measurements are recorded on magnetic tape for analysis.

The orbit plane precession is useful for sampling all local times of the day. Consider a non-rotating earth, with the orbit plane intersecting the equator at Ω longitude (as well as $\Omega + 180^0$). The orbit precession results in a slow change of Ω depending on orbit inclination, i, and radius, r_s,

$$\frac{d\Omega}{dt} = - J\left(\frac{r_s}{r_e}\right)^{3.5} \sin i \qquad (10)$$

$J = 10.05^0/\text{day}$

In this system the sun moves west to east about 1^0 per day.

$$\frac{d\phi_{sun}}{dt} = 360^0/365.25 \text{ day} \qquad (11)$$

The local time, t_L, of the orbital crossing is then the difference of ϕ_{sun} and Ω with suitable factors of 2π removed:

$$t_{local} = \Omega - \phi_{sun} \qquad (12)$$

The time interval, t, for combining many individual measurements is chosen here to be 30 days. This is longer than the daily or weekly weather changes and shorter than seasonal changes. As envisioned now the earth radiation budget measurements will be used for climate studies which consider month time scales. This scale has the advantage that all geography will be sampled many times (at least four) in each latitude zone, because of the fast rotation of the earth.

The problem of sampling all local times is more difficult. Crudely in a period T, all local times pass under one satellite in latitude zones from +i to -i.

$$\tau_{all} = \left| \frac{2\pi}{d\lambda_L/dt} \right| = \left| \frac{2\pi}{\frac{d\Omega}{dt} - \frac{d\lambda_{sun}}{dt}} \right| \qquad (14)$$

This period is very long for high inclination orbits reaching 6 months for 90^0 inclinations. This problem was recognized at the inception of this project so multiple satellite systems have always been considered.

A simple way to look at the inclination selection problem would be to examine how a system samples the latitude, local time space in a month. That is, the percentage of all local times as observed by the system at each latitude in a measurement interval. This is necessarily a qualitative examination as a simple area weighting of each latitude zone would underestimate the importance of the polar regions in the weather. Also the sensor does not make a measurement just at one local time point but over some region. For this discussion we assume measurements cover a region as big as the half power area of the sensor. This is a circle of 7.2^0 radius for a spherical sensor at 800 km above the surface. This translates to plus or minus one half hour at the equator.

As two or more satellites precess about, there is a large variation in the coverage as the orbit planes move relative to each other. Figure 5 shows the percent coverage with each latitude zone weighted equally. There is smaller area at high latitudes but the sensor looks at wider local time regions. This number implies that each zone is equally important as the weather is driven by north-south differences rather than area differences.

The perfect sensor system would look at all local times at all latitudes equally often. Incidently, three 80^0 inclined orbits in phase do this in a month. But the simple satellites considered probably will not be launched accurately enough to maintain equal spacing in Ω of the satellites.

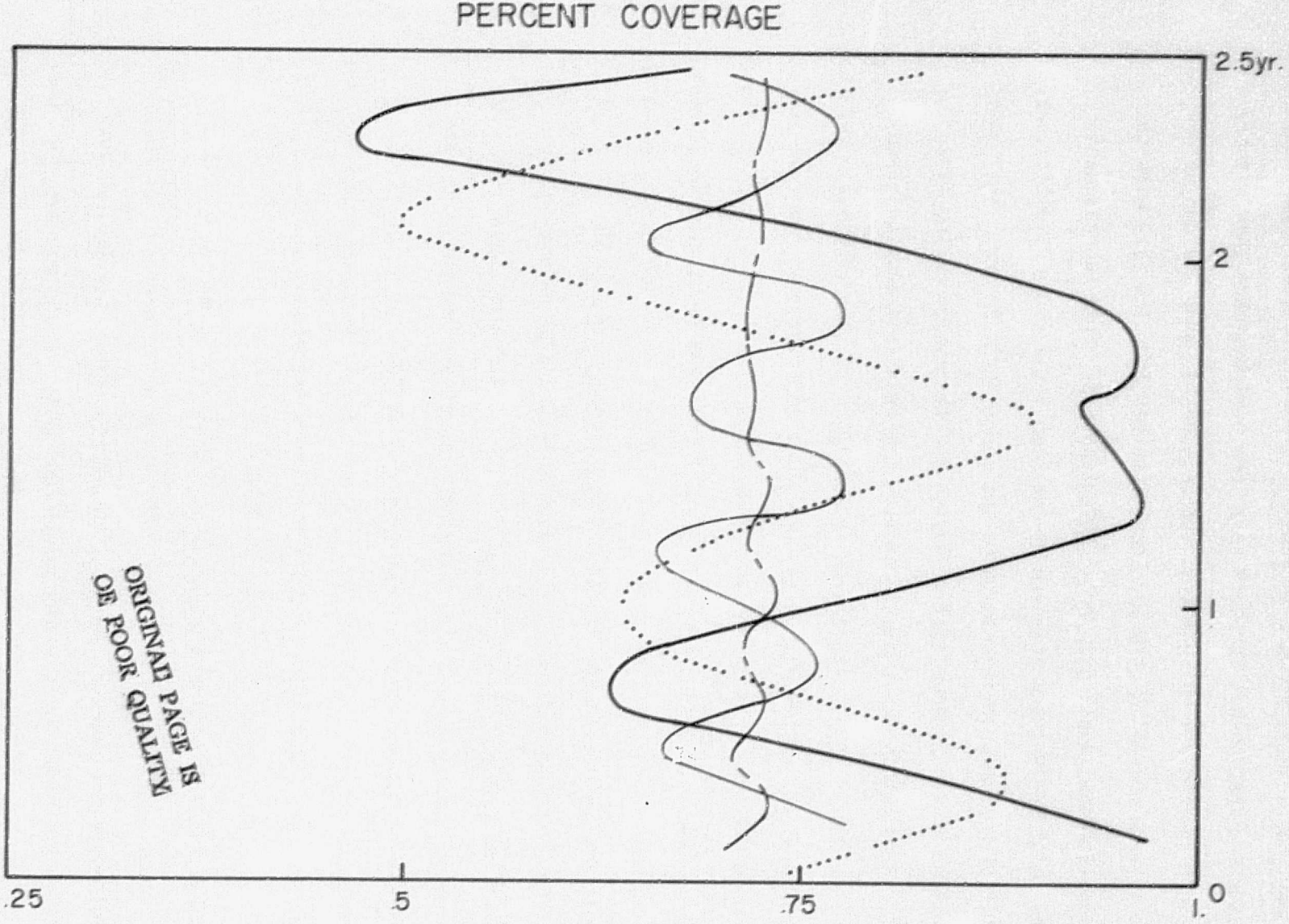

Qualitative estimate of effectiveness of different orbit inclinations in sampling local time and space for 2.5 years.

FIG. 5

For two randomly processing satellites launching them with almost the same inclination will produce very long periods (more than a year) with very inefficient measurements (see Figure 5), when the two satellites will be observing only one local time region. The pair with the best qualitative sampling is 50^{o} + 80^{o}, Figure 5. This is reasonable as the polar regions are observed by the high inclination satellite and a wide local time region is sampled by the lower inclined one. The "best" is defined as the minimum quality factor for the system during five years. This result is in agreement with the results discussed below of the best pair found with a detailed analysis of simulated measurements. Two sun synchronous satellites produce a quality nearly as large as the minimum of the 80, 50 set, but they sample the same local time space region at all times. These two consistantly skip the same local time space area leaving events in this area unrecorded. Table I shows various sytems with the minimum quality factor calculated for them.

For more than two satellites this quality factor becomes very insensitive to small changes in inclination. Almost all local times are sampled at least once with the number of repetitions now becoming more important. The more complex simulation discussed below is necessary to distinguish between these systems. Also, the anlysis below emphasizes the energy fluxes rather than just the geometrical aspects.

IV. ANALYSIS OF MANY INDIVIDUAL MEASUREMENTS

The analysis of large groups of measurements is the most poorly understood problem discussed here. Above any given geographical region measurements are taken at varying frequencies during the day. Unfortunately these are not distributed at random during the day but are made generally with large gaps in local time. This indicates the need for some interpolation procedure to fill in the gaps.

Table I. Minimum Coverage

Fraction of Local Time, Space

	Regions Sampled	
	Twice	Eight times
$90^{o} + 30^{o}$	.64	.42
$90^{o} + 40^{o}$	.68	.41
$90^{o} + 50^{o}$	.70	.40
$90^{o} + 60^{o}$	.69	.42
$80^{o} + 30^{o}$	.67	.45
$80^{o} + 40^{o}$	.70	.45
$80^{o} + 50^{o}$	.70	.46
$80^{o} + 60^{o}$	.68	.46
$80^{o} + 90^{o}$	.54	.45
$80^{o} + 70^{o}$	.50	.48
$78^{o} + 30^{o}$	.66	.45
$78^{o} + 40^{o}$	.68	.45
$78^{o} + 50^{o}$	.68	.45
$78^{o} + 60^{o}$	.67	.45
$78^{o} + 70^{o}$	.60	.47
$80^{o} + 78^{o}$	.52	.45
$98^{o} + 98^{o} + 30^{o}$	.69	.47
$98^{o} + 98^{o} + 40^{o}$	.74	.47
$98^{o} + 98^{o} + 50^{o}$	.75	.45
$98^{o} + 98^{o} + 60^{o}$	.74	.45
$98^{o} + 98^{o} + 70^{o}$	.68	.48

The number represents the fractional area coverage on a rectangular map of the globe with equal length latitude zones with longitude representing local time.

The reflected power component is the most difficult as it varies from zero to several hundred watts depending on sun angle (Fig. 6). A first order prediction of this variation can be made with a diffuse reflecting earth. Three methods of fitting to this diffuse form factor have been tried with varying success. The variation in the emission component is small enough so that a simple average is adequate.

These analysis methods were developed to intercompare various orbital systems. To minimize the effect of the analysis scheme a reference measurement set was generated with uniform space and time sampling. Using a specific analysis scheme on the reference set and comparing the results to each specific system of sensors measures the accuracy of the system. There are bias errors introduced by the analysis schemes which ultimately can be removed with better techniques. For the reference set a measurement is taken at 18 local times above 748 geographical regions on the earth for each day of the measurement interval. The regions are chosen with approximate equal area corresponding to squares 7.5^{o} by 7.5^{o} at the equator. This is similar to the results of hundreds of satellites flying in random orbits all at the same altitude.

It is clear that some averaging in space as well as time is needed to reduce the local fluctuations and get a reasonable sample of all possible weather events. The weather patterns when averaged in time show a strong zonal homogeneity. So zonal averaging of the measurements is a reasonable

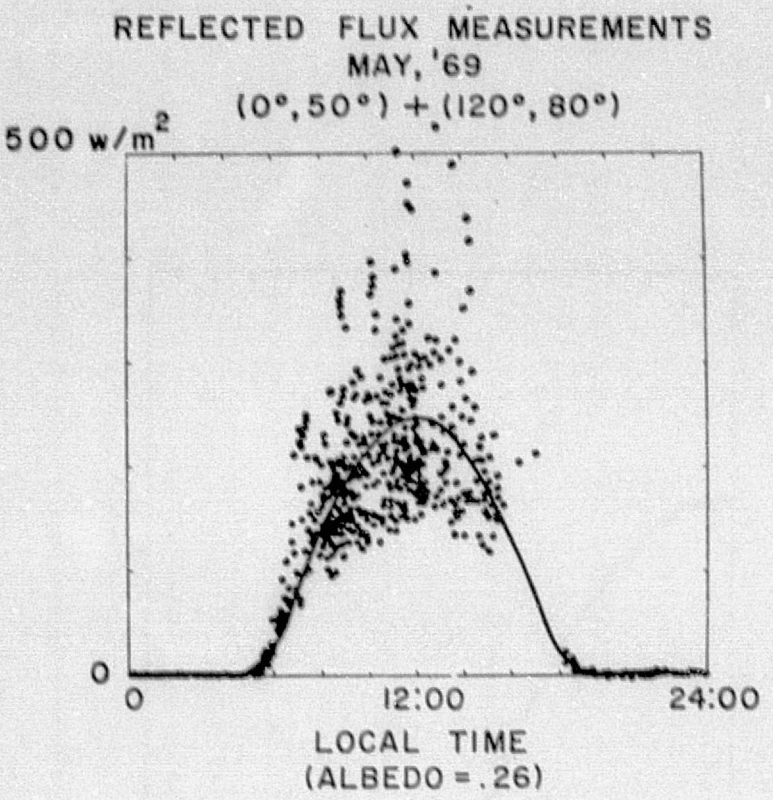

17.5° S TO 15° S

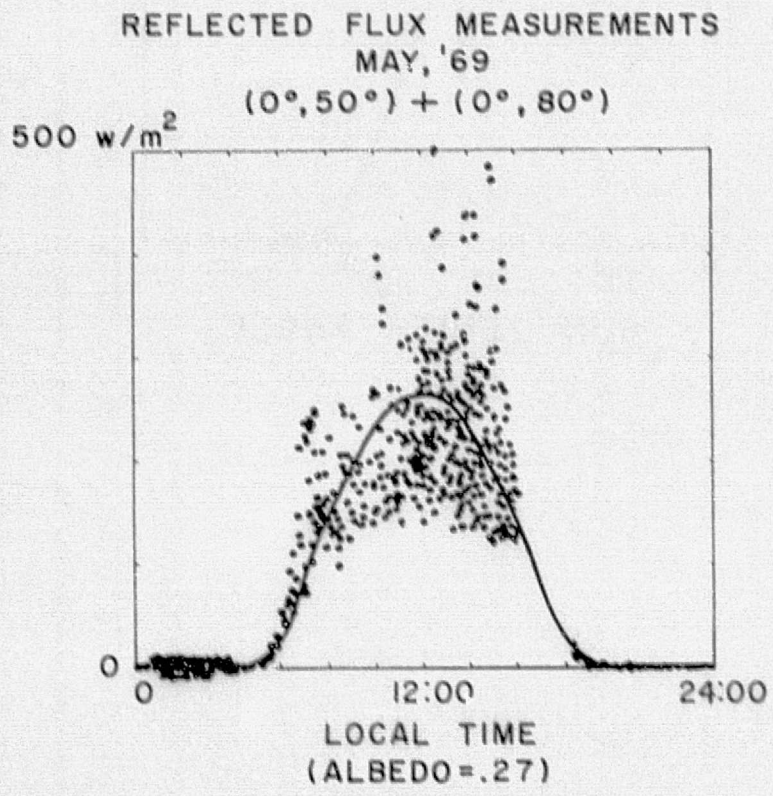

FIG. 6 Measurements made by two different orbit pairs in the latitude zone 17.5°S to 15°S.

Top 50° inclined Ω = 0° and 80° inclined Ω = 120°

Bottom 50° inclined Ω = 0° and 80° inclined Ω = 0°

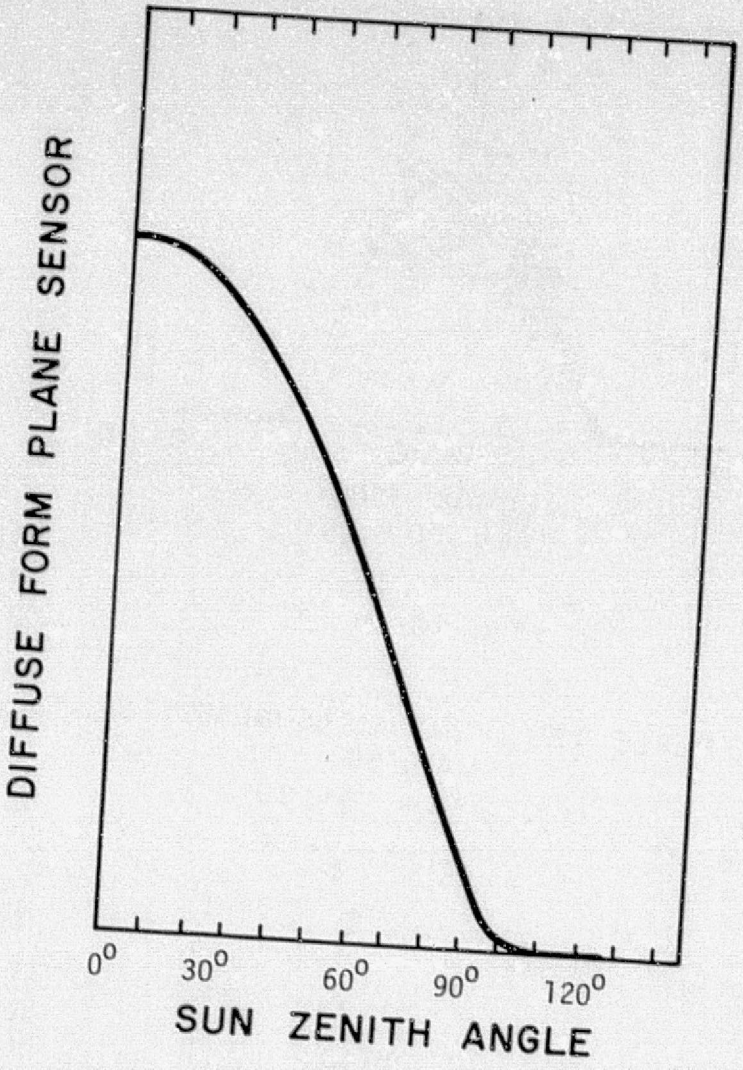

FIG. 7

method of smoothing fluctuations. It must be realized that any system will miss some events and misinterpret others. It is assumed that missing measurements will be uncorrelated with surface events.

We list below several methods of analyzing the individual measurements which all involve some form of space and time averaging.

a) The crudest analysis technique is to simply average all measurements in a latitude zone irrespective of location and local time.

$$[m(\theta_s)] = \frac{\sum_{k=1}^{K} m_k(\theta_s, \phi_s)}{K} \tag{15}$$

where K includes all measurements in a latitude zone around θ_s.

This works fairly well for the long wave component. But ignoring observational biases in local time for the reflected produces useless results. Figure 6 shows reflected power measurements for two satellites in one latitude zone for a month. The large diurnal variation in the reflected component makes neglecting the gaps untenable.

b) One might first segregate the measurement into local time intervals within the zone. Average those in a local time bins and then average the bins results ignoring the gaps (Eq. 16). This removed any inhomogeneities in measurement frequency except it still ignores the gaps.

$$[m(\theta_s, \phi_s)] = \sum_{j}^{J} \frac{\sum_{k=1}^{K} m_k(\theta_s, \phi_s, t_{i_j})/K}{J} \tag{16}$$

where the sums in the numerator include only measurements in the jth local time interval.

c) The only way to span the gaps is to predict the average measurement within the gaps. Even a crude prediction is better than none. By assuming a diffuse constant reflector on the earth's surface function, f, of sun angle is produced which is similar to the measurement. Figure 7 shows f vs. sun angle. A simple one parameter fit of the measurements in a zone and the diffuse form produce something like a zonal albedo, A_c. Here a two parameter fit has been used extensively generating an anisotropic factor, B_c, as well.

$$\sum_k [(A_c + B_c \sin t_L)\, f(t_L) - n_k(t_{Lk}, \theta_s, \phi_s)]^2 = k\sigma^2 \qquad (17)$$

Summing over all measurements in a latitude zone. Minimizing σ^2 predicts A_c and B_c.

This is essentially the technique used in the past for sun synchronous measurements. Only one local time was available so a simple diffuse normalization predicts $A_{(sunsync)}$.

$$A_{sunsync} = \frac{1}{I} \sum_{i=1}^{L} n_i / f(t_i) \qquad (18)$$

A_c can be converted to reflected power by integrating f over the day (Eq. 19).

$$[n(\theta_s)]_c = A_c \int F(t_L)\, dt_L \Big/ \int dt_L \qquad (19)$$

Notice that the average of $B_c f \sin t_L$ is zero as the sin is antisymmetric. The B_c given a measure of the diurnal variation of A_c. No attempt was made to use this technique on the emitted powers as there is no obvious corresponding f function. The

results of this technique are discussed below.

The obvious improvement in this method is a more subtle calculation of f using bidirectional reflection models. This was not tried as only two reflection models were used in the program and it would be too easy to plug them back in. The real earth has more unpredictable reflection characteristics.

d) A more comprehensive three dimensional separation technique is to segregate the measurements for a month into local time and space volumes. All the measurements above one of 748 equal area regions are averaged together if they fall in the same local time segment.

$$<m(\theta_i, \phi_j, t_\ell)> = \sum_k m_k(\theta_s, \phi_s, t_L)/K$$

$$\text{if } (\theta_i < \theta_s < \theta_{i+1});\ (\phi_j < \phi_s < \phi_{j+1}),\ (t_\ell < t_L < t_{\ell+1}) \tag{20}$$

If there are systematic variations during the day and these variations change from one local time to another, this technique should handle them the best. It weighs each local time segment equally irrespective of the number of measurements within the segment.

The daily average infrared partial average, $< m >$, can be produced by a simple average ignoring time gaps. Then the zonal average can be taken by summing over j again ignoring gaps in longitude. The gaps in the reflected partial average again are much more serious. The gaps can best be filled as discussed in technique c.

$$\langle n_{ij} \rangle = \langle A_{ij} \rangle \int F(t_i)\, dt_L / \int dt_L \qquad (21)$$

Getting $\langle A_{ij} \rangle$ from

$$\sum_k \left[\langle A_{ij} \rangle \int_{t_k}^{t_{k+1}} f(t_L) dt_L - \langle n_{ij\ell} \rangle \right]^2 = k\sigma^2 \qquad (22)$$

The zonal average of $< n >$ is then just the sum of occupied bins;

$$[\langle n\ (\theta_i) \rangle\ ] \sum_j \langle n_{ij} \rangle / J \qquad (23)$$

This technique has also been used extensively with the results discussed below. Again this produces an effective albedo at the satellite which is converted to reflected power. The major problem here is the poor statistics as many space, time volumes will be empty and few will have more than ten measurements per month. This shows the advantage of method c with its better statistics.

e) A combination of c and d would be a two dimensional segregation in local time and latitude ignoring longitude before doing the fit. This technique has not been tried but it may still suffer from gaps in some local time segments.

f) An entirely different technique for handling the reflected measurement is to form ratios of n to f and average these individual 'albedoes'. This method recognizes that there is a large variation during the day of n but a smaller variation in albedo.

$$\tilde{a} = \sum_k n_k / f_k \qquad (24)$$

k indicates of all measurements in any space-time volume. This assumption is poor but even worse, averages should not be made of albedoes but of powers. This method is very bad except for combinations of sun synchronous orbits where only two or three local items are available in any region.

g) So far the methods listed divide the measurements into local time space regions and then average. This is somewhat artificial as the field of view has a great circle arc radius of about 25^{o}. A more reasonable procedure might expand the measurements into a set of orthogonal functions like spherical harmonics, $Y_i^j(\theta,\phi)$

For the infrared local time can be ignored so the spherical harmonic coefficients can be found by a least squares fitting.

$$\frac{\partial}{\partial b_{ij}} \sum_k \left[m_k(\theta_s,\phi_s) - \sum_{i=o}^{I} \sum_{j=-i}^{i} Y_i^j(\theta_s,\phi_s) b_{ij}\right]^2 = 0 \qquad (25)$$

which implies b_{ij}.

In the reflected measurements some local time variation is necessary. A reasonable procedure is to again use the diffuse function f.

$$\frac{\partial}{\partial a_{ij}} \sum_k \left[n_k(\theta_s,\phi_s,t_L) - \sum_{i=o}^{I} \sum_{j=-i}^{i} Y_i^j(\theta_s,\phi_s) \cdot a_{ij}\, f(t_{Lk})\right]^2 = 0 \qquad (26)$$

which implies a_{ij}.

Perhaps 100 coefficients are significant with the others down in the noise of atmospheric features or of the measurement noise.

h) A simpler procedure utilizes the strong zonal symmetry of the climate. Retaining only the zonal coefficients (a_{io}, b_{io}) which reduces the equations to coefficients of Legendre polynomials.

$$\frac{\partial}{\partial b_{io}} \sum_k [m_k(\theta_s,\phi_s) - \sum_{i=o}^{I} b_{io} P_i(\theta_s)]^2 = 0 \qquad (27)$$

$$\frac{\partial}{\partial a_{io}} \sum_k [n_k(\theta_s,\phi_s,t_L) - \sum_{i=o}^{I} P_i(\theta_s)\, a_{io} f(t_L)]^2 = 0 \qquad (28)$$

These methods are most interesting in light of the deconvolution discussion given below. Depending on certain assumptions about emission model and reflectance models, Legendre polynomials, P, and spherical harmonics, Y, are eigen functions of the measurement operator. One can thus arrive at an integral equation relating the coefficients to a similar expansion of the surface features.

In summary, even more complex techniques will be needed to handle the real data. There will be variations in orbit altitude which must be removed. The diffuse reflection form f could be altered to include bidirectional reflectance effects and orbit radius changes. Also crude predictions of diurnal variations in reflected and infrared might improve the analysis. This work will be done when a commitment to fund a specific satellite system is made. The three methods used here are sufficiently sensitive to do the reproducibility studies attempted here.

V. ACCURACY AND REPRODUCIBILITY RESULTS

Comparisons between the reference measurement set at satellite altitude analyzed with one of the methods above with a system of satellites analyzed in the same manner gives a measure of the accuracy of the system. The variations in different system accuracies result from sampling variation. A measure of reproducibility is provided by a comparison of different sets of Ω_o's within a system of particular inclinations. It is felt by the authors that the intercomparisons indicate the approximate reproducibility of the different systems and the best system with inclinations estimated to $\pm 5^o$. There are unresolved systematic errors between different analysis schemes. These arise from numerical inaccuracies and perhaps from insufficient local time resolution in the reference set. The amount of computer time was prohibitive for testing to find the source of these systematic errors. Finer resolution in optimizing the inclinations of a number of satellites will require better analysis schemes and a better reference.

For the discussion below a system is any set of satellites with one group of specific inclinations. Table II shows all the individual orbit parameters used. The different sets have orbits with the same inclinations but different right accessions, Ω, at launch. Small inaccuracies in launch altitude and inclination will result in uncertain precession rate. Thus, with the long life time envisioned for the measurement system, the Ω's become unpredictable after a few years.

More than 100 combinations have been analysed with method d. These show the importance of at least two satellites in each system. The number of cases considered was limited by computer time. The variations in the results of this analysis scheme were essentially the same as the results of method e, which follows.

Table II. Orbits Generated

Orbit radius - 7178 km (800 km above surface)

	i (inclination)	Ω_o (equator crossing)	
1.	15°	334°	
2.	30°	179°	
3.	30°	269°	
4.	40°	59°	
5.	40°	149°	
6.	50°	359°	
7.	50°	89°	
8.	60°	209°	
9.	60°	299°	
10	80°	239°	
11.	80°	359°	
12.	80°	119°	
13.	80°	224°	
14.	90°	314°	
15.	90°	14°	
16.	90°	74°	
17.	90°	344°	
18.	90°	44°	
19.	90°	104°	
20.	98.6°	72°	Sun sync 3:00 local
21.	98.6°	267°	Sun sync 10:00 local
22.	98.6°	27°	Sun sync 12:00 local
23.	98.6°	297°	Sun sync 18:00 local
24.	120°	29°	

A. ERROR MEASURE

Method e has been run for several thousand combination sets and thus for several hundred systems. Figures 8-12 and Table III, IV, V, VI show several cases including both the worst and best systems discovered. The "errors" are crudely represented as the standard deviation between the reference and the various systems measurements, e_i. This standard deviation is the root mean square deviation between the reference zonal averages and each of the zonal averages of the sets within the system, (eg., 29).

$$e_i = \left\{ \frac{\sum_j [m_j(\theta_i) - R(\theta_i)]^2}{J-1} \right\}^{1/2} \qquad (29)$$

$M_j(\theta_i)$ = i^{th} latitude zonal result of the analysis of the j^{th} combination of Ω's in a system.

$R(\theta_i)$ = reference results in the ith latitude zone.

Figures 8-12 show some plots of zonal averages compared to the reference. The dots show the result of each set. The dots dispersion is representative of the error which will occur some time during an experiment using the particular system. An internal consistency or reproducibility measure also appears in the tables, it results from replacing R with the average of m for the set.

A similar error estimate can be computed for a set of polynomial coefficients. Table IV and V show some polynomial error measures. This does not give quantitative results but allows one to intercompare different systems on a global scale.

Table VI shows error measures for a spherical sensor system. It agrees with table III in most details. The sphere and the plate do not give significant sampling differences at the scales under study (see below).

ZONAL AVERAGE MEASUREMENTS

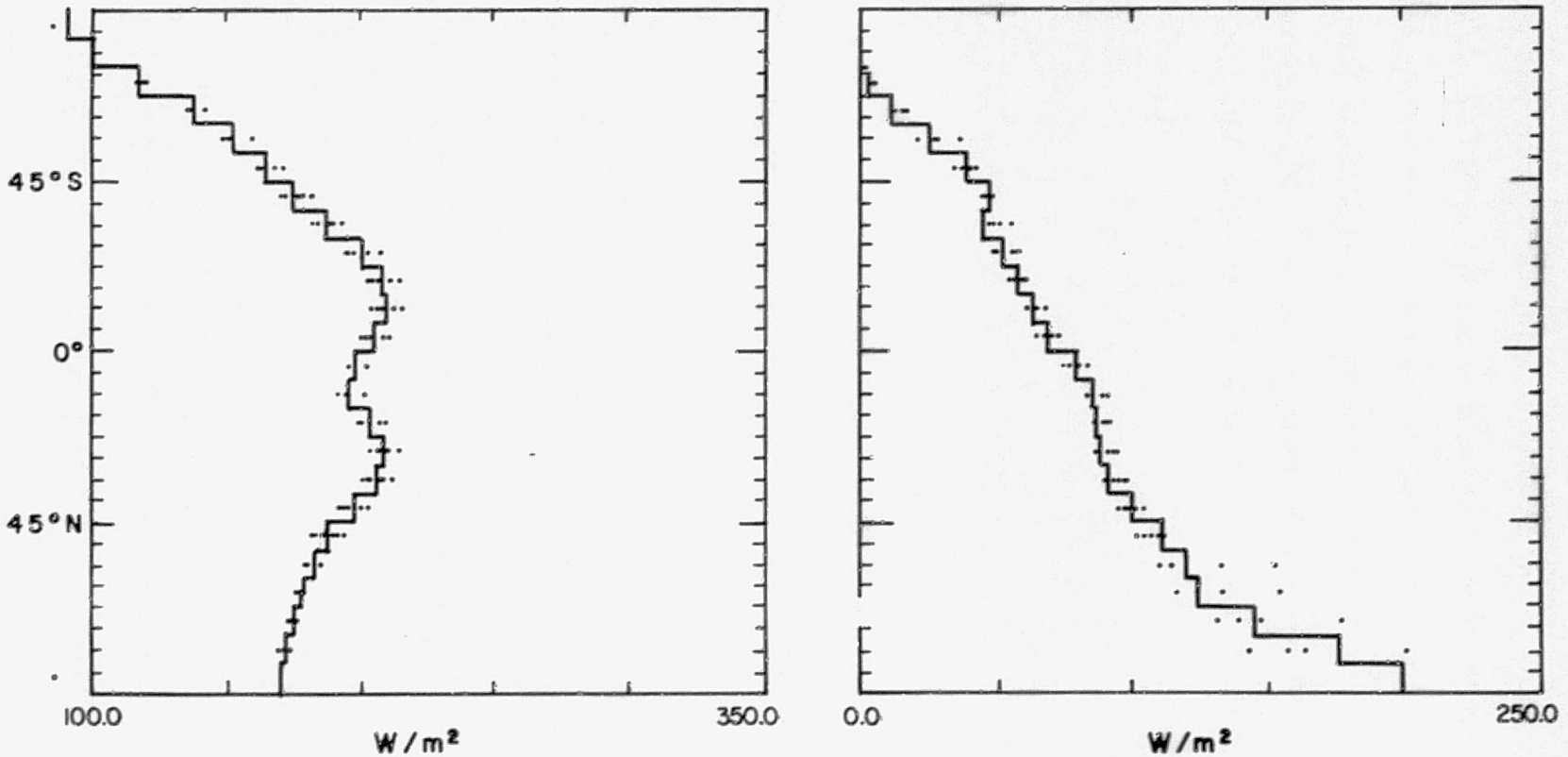

EMITTED FLUX, FLAT PLATE

REFLECTED FLUX, FLAT PLATE

• 80° + 50° RESULTS

—— REFERENCE MEASUREMENTS

THE DISPERSION OF THE DOTS IS CAUSED BY IMPERFECT LOCAL TIME SAMPLING.

FIG. 8

ZONAL AVERAGE MEASUREMENTS

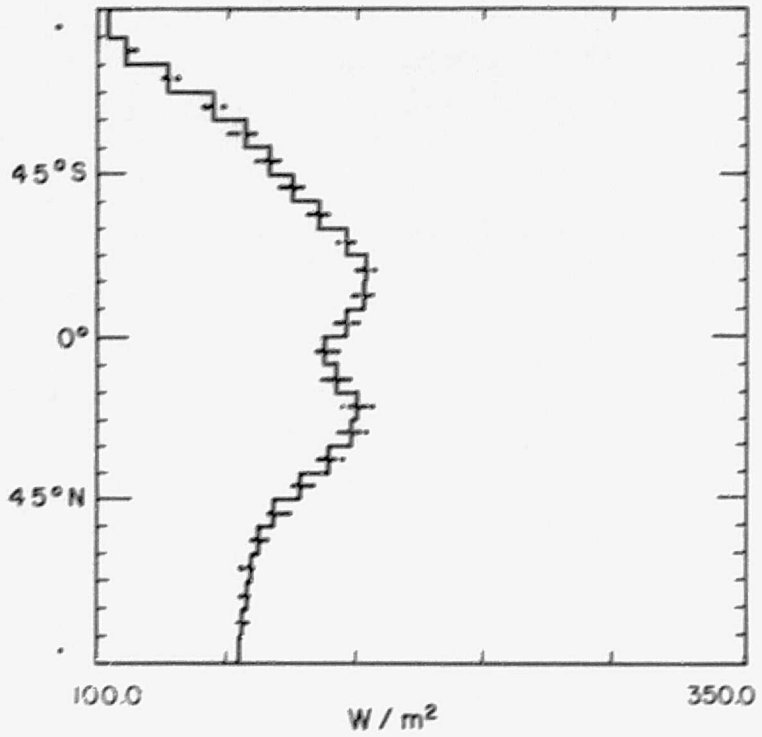

EMITTED FLUX AT SATELLITE
FLAT PLATE

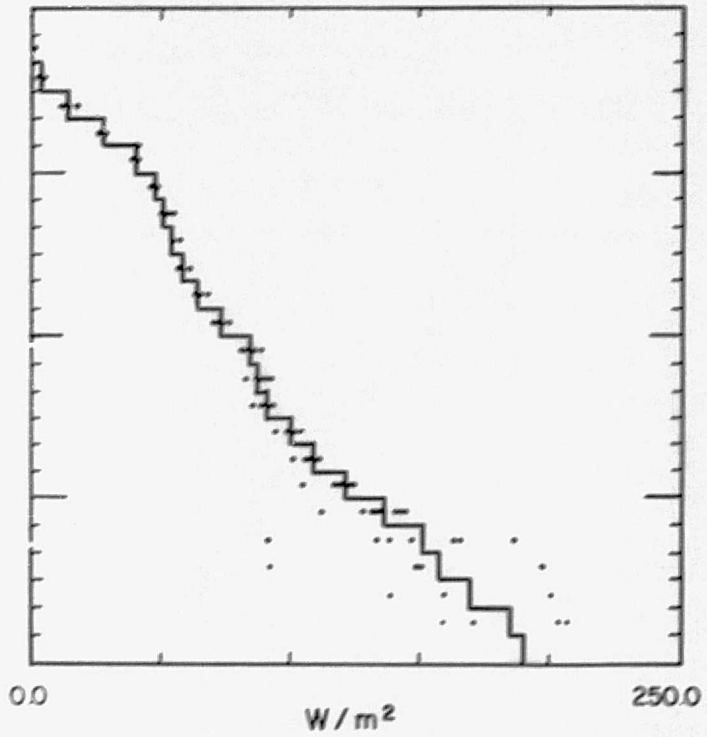

REFLECTED FLUX AT SATELLITE
FLAT PLATE

• 80° + 60° + 50° SETS

—— REFERENCE MEASUREMENT

FIG. 9

ZONAL AVERAGE MEASUREMENTS

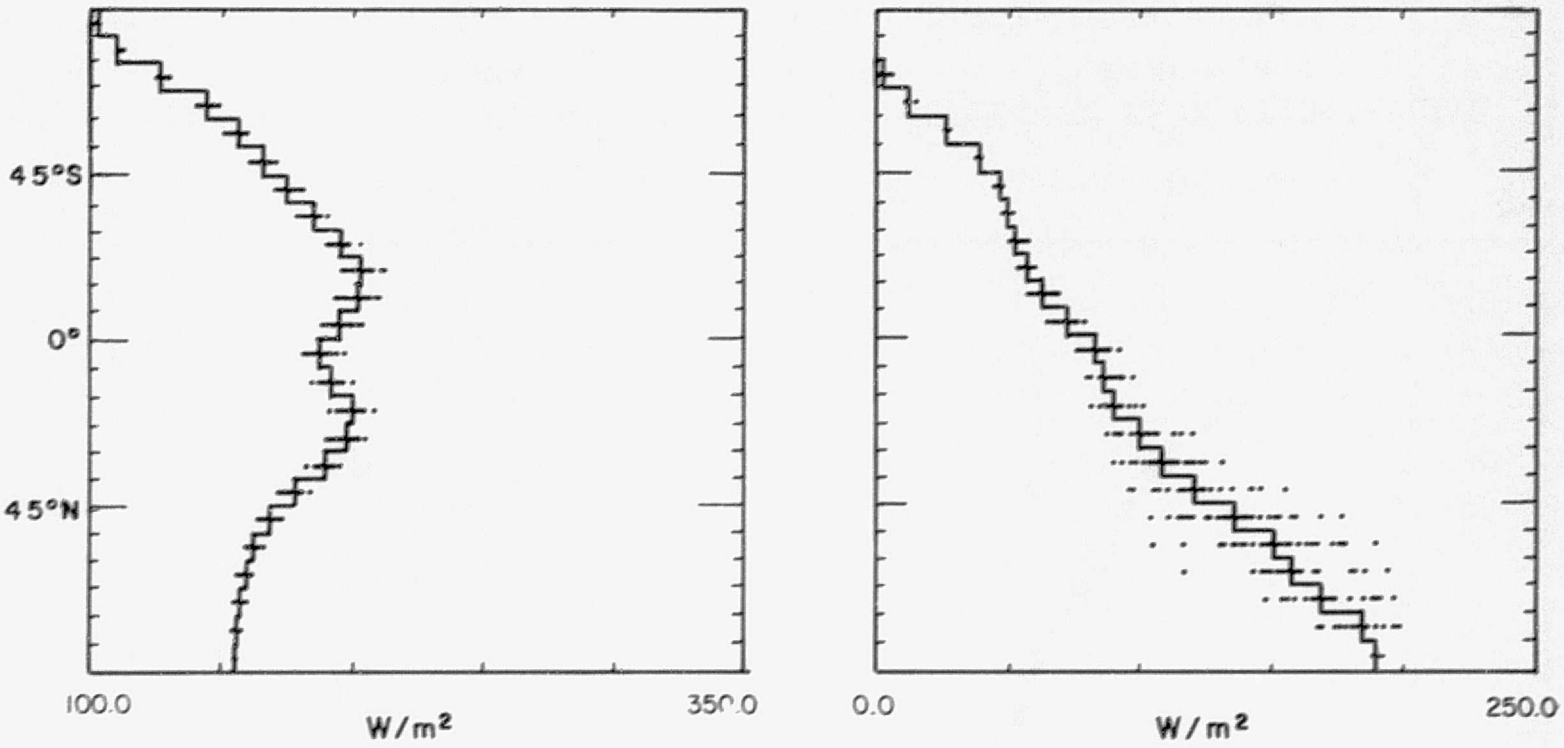

EMITTED FLUX AT SATELLITE
FLAT PLATE

REFLECTED FLUX AT SATELLITE
FLAT PLATE

• 90°+80°+50° SETS
—— REFERENCE MEASUREMENT

FIG. 10

ZONAL AVERAGE MEASUREMENTS

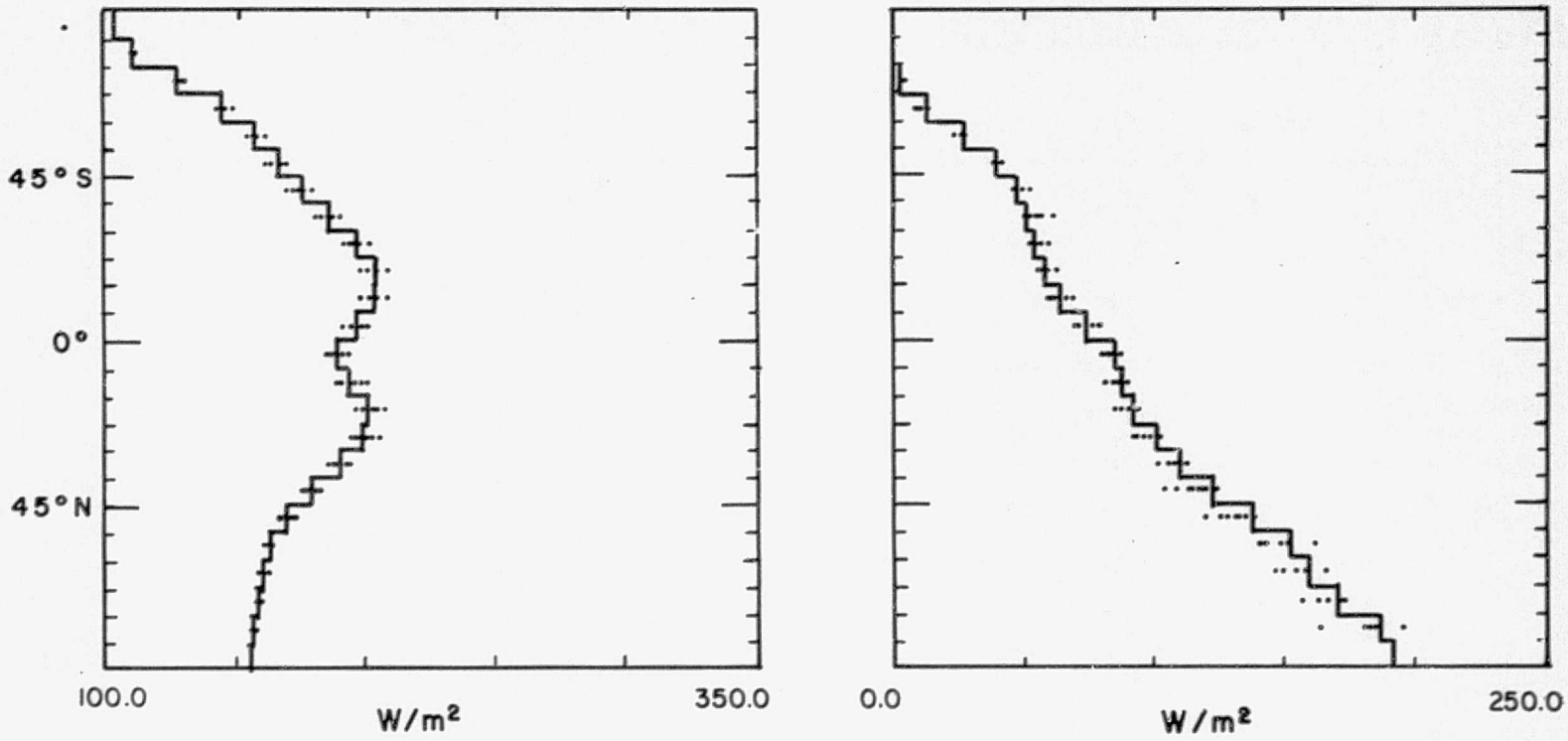

EMITTED FLUX AT SATELLITE
FLAT PLATE

REFLECTED FLUX AT SATELLITE
FLAT PLATE

• TWO SUNSYNCHRONOUS PLUS 50°

—— REFERENCE MEASUREMENT

FIG. 11

LEGENDRE POLYNOMIAL COEFFICIENTS OF MEASUREMENT

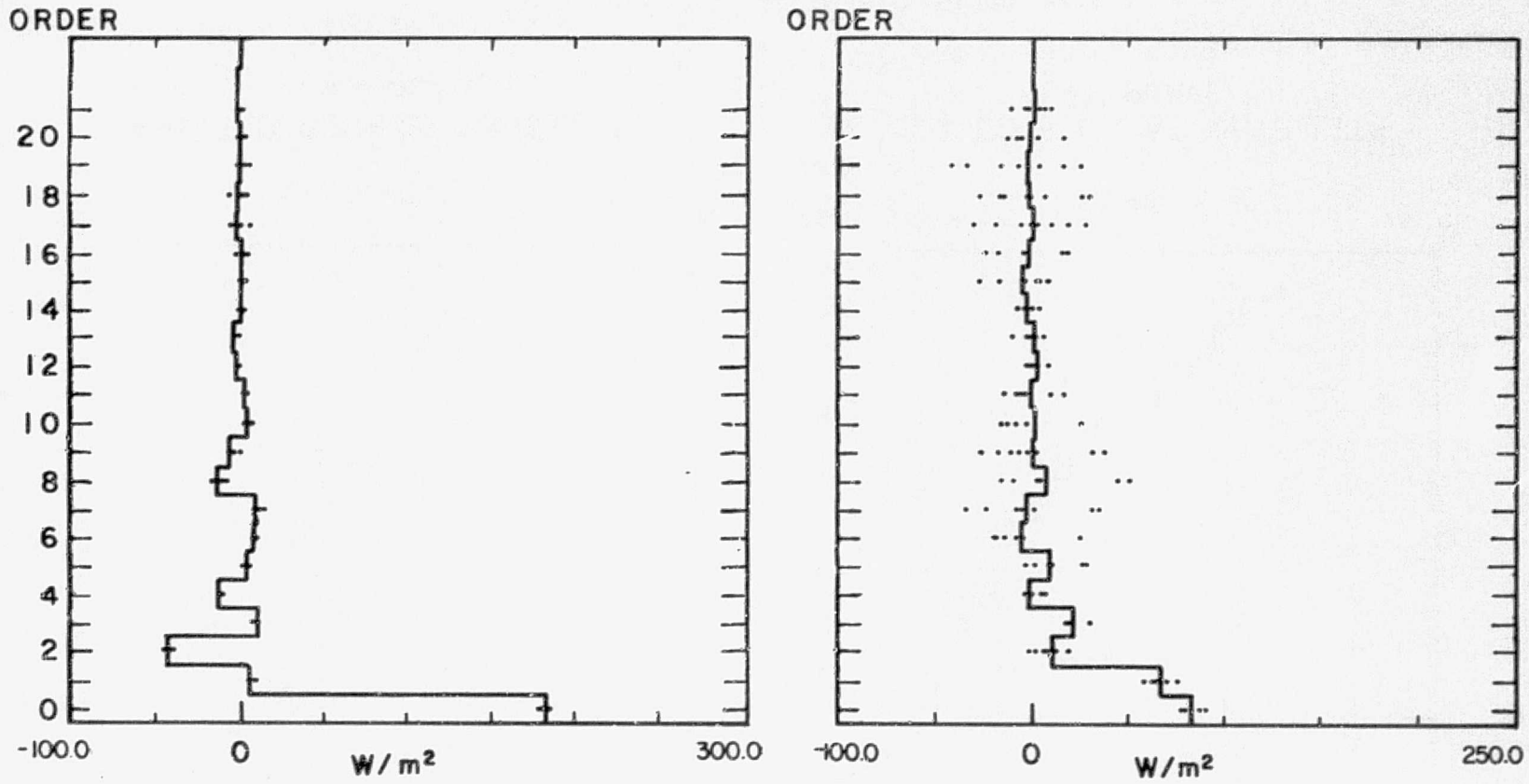

EMITTED FLUX, FLAT PLATE

REFLECTED FLUX, FLAT PLATE

• 80°+50° RESULTS

—— REFERENCE MEASUREMENTS

FIG. 12

Table III.

Emitted Flux Error Measure
Zonal Averages
Flat Plate
W/M^2

+	Relative to Reference Accuracy 30	40	50	60	Internal Consistency Reproducibility 30	40	50	60
80	4.13	3.49	3.34	3.54	3.91	3.50	3.30	3.56
90	4.64	3.90	3.83	3.92	4.60	3.96	3.79	4.03
98.6	4.53	3.82	3.69	3.85	4.53	3.96	3.80	4.06
80+40	3.15				2.81			
80+50	2.81	2.60			2.46	2.50		
80+60	2.88	2.67	2.59		2.52	2.56	2.45	
90+40	3.42				3.18			
90+50	3.06	2.90			2.80	2.82		
90+60	3.05	2.87	2.85		2.82	2.82	2.74	
90+80	3.52	2.85	3.28	3.40	3.25	3.15	3.13	3.31
98.6+40	3.37				3.12			
98.6+50	2.97	2.80			2.73	2.77		
98.6+60	3.05	2.82	2.76		2.82	2.80	2.72	
98.6+80	3.53	3.25	3.23	3.40	3.22	3.15	3.12	3.31
98.6+90	3.66	3.41	3.44	3.55	2.48	3.36	3.36	3.55
98.6+98.6	2.69	2.61	2.69	2.50	2.69	2.61	2.75	2.33
80+80+50	2.40	2.23		2.30	1.96	2.04		2.03
80+80+80	2.45	2.26	2.20		1.73	1.89	1.77	
80+80+120			2.34				1.94	
90+90+50	2.62	2.54			2.36	2.42		
90+90+60	2.66	2.56	2.59		2.44	2.48	2.45	
90+90+120			3.15				2.39	
98+98+50	2.42	2.32			2.19	2.26		
98+98+60	2.52	2.40	2.34		2.26	2.34	2.28	
98+98+98	2.22	2.12	2.01	2.07	1.97	2.11	2.02	2.13
98+98+120			2.78				2.23	

Orbit Inclination Combinations
Column headings and row prefixes indicate inclinations included.

Table IV.

Reflected Flux Error Measure
Polynomial Representation
Flat Plate
W/M^2

+	Relative to Reference Accuracy 30	40	50	60	Internal Consistency Reproducibility 30	40	50	60
80	8.00	6.20	5.82	5.66	8.30	6.47	6.06	5.80
90	8.09	4.78	4.02	4.10	7.63	4.71	3.87	4.21
98	36.9	25.6	12.3	7.22	30.4	23.4	12.3	7.18
80+40	6.21				6.25			
80+50	5.97	5.91			6.02	5.96		
80+60	5.47	4.85	5.30		5.49	4.92	5.33	
90+40	4.74				4.56			
90+50	3.91	3.69			3.69	3.48		
90+60	4.02	3.49	3.12		4.01	3.44	3.03	
90+80	4.21	2.98	2.59	3.03	4.18	2.90	2.47	3.00
98+40	25.7				22.5			
98+50	12.5	12.5			12.0	12.1		
98+60	7.18	6.90	6.70		6.99	6.77	6.52	
98+80	4.93	3.87	3.08	3.47	4.82	3.80	2.91	3.26
98+90	4.49	3.15	2.70	2.97	4.47	3.07	2.55	2.96
98+98	3.39	2.74	2.37	2.67	3.34	2.53	1.91	2.30
80+80+50	1.55	1.61		1.83	1.40	1.40		1.67
80+80+80	1.10	0.91	0.85	1.59	0.65	0.53	0.57	0.94
80+80+120			2.10				1.07	
90+90+50	1.43	1.48			1.20	1.20		
90+90+60	1.35	1.46	1.24		1.18	1.18	1.00	
90+90+120			1.38				1.04	
98+98+50	1.88	1.72			1.53	1.50		
98+98+60	2.03	1.76	2.05		1.91	1.62	2.00	
98+98+98	1.37	1.27	0.96	1.44	1.00	0.85	0.60	1.12
98+98+120			1.74				1.11	

Orbit Inclination Combinations
Column headings and row prefixes indicate inclinations included.

Table V.

Emitted Flux Error Measure
Polynomial Representation
Flat Plate
W/M^2

	Relative to Reference Accuracy				Internal Consistency Reproducibility			
+	30	40	50	60	30	40	50	60
80	2.08	1.65	1.55	1.64	1.97	1.66	1.52	1.64
90	1.97	1.68	1.69	1.72	1.97	1.73	1.67	1.78
98.6	2.17	1.77	1.71	1.73	2.16	1.80	1.76	1.83
80+40	1.55				1.37			
80+50	1.66	1.29			1.29	1.25		
80+60	1.52	1.25	1.28		1.32	1.23	1.20	
90+40	1.44				1.35			
90+50	1.27	1.25			1.19	1.23		
90+60	1.27	1.23	1.23		1.19	1.23	1.20	
90+80	1.51	1.23	1.45	1.50	1.41	1.39	1.39	1.47
98.6+40	1.60				1.46			
98+50	1.72	1.42			1.39	1.38		
98+60	1.54	1.30	1.31		1.39	1.30	1.29	
98+80	1.72	1.51	1.47	1.55	1.56	1.44	1.43	1.50
98+90	1.57	1.49	1.52	1.57	1.51	1.48	1.49	1.57
98+98	1.52	1.37	1.30	1.36	1.42	1.34	1.32	1.38
80+80+50	1.39	1.06		1.12	1.04	0.99		0.99
80+80+80	1.22		1.01		0.92		0.82	
80+80+120			1.22				0.90	
90+90+50	1.10	1.10			1.02	1.06		
90+90+60	1.11	1.29	1.28		1.04	1.28	1.22	
90+90+120			1.38				1.06	
98+98+50	1.39	1.12			1.12	1.09		
98+98+60	1.27	1.11	1.10		1.13	1.08	1.08	
98+98+98	1.10	1.02	0.91	0.97	0.99	0.97	0.93	0.97
98+98+120			1.37				1.00	

Orbit Inclination Combinations
Column headings and row prefixes indicate inclinations included.

Table VI.

Emitted Flux Error Measure
Zonal Averages
Spherical Sensor
W/unitsphere

+	Relative to Reference Accuracy 30	40	50	60	Internal Consistency Reproducibility 30	40	50	60
80	5.83	4.92	4.72	4.99	5.52	4.95	4.66	5.02
90	6.52	5.48	5.39	5.50	6.46	5.57	5.32	5.67
98.6	6.39	5.39	5.21	5.43	6.40	5.59	5.36	5.74
80+40	4.44				3.97			
80+50	3.96	3.66			3.48	3.53		
80+60	4.07	3.77	3.66		3.56	3.63	3.45	
90+40	4.81				4.48			
90+50	4.29	4.06			3.93	3.96		
90+60	4.29	4.04	4.00		3.97	3.97	3.85	
90+80	4.95	4.57	4.62	4.78	4.58	4.45	4.41	4.67
98+40	4.81				4.48			
98+50	4.18	3.95			3.86	3.92		
98+60	4.25	3.99	3.89		3.92	3.96	3.84	
98+80	4.98	4.58	4.57	4.79	4.54	4.45	4.41	4.67
98+90	5.15	4.80	4.85	5.00	4.90	4.74	4.74	5.00
98+98	4.06	3.80	3.69	3.88	3.84	3.80	3.69	3.80
80+80+50	3.39	3.15		3.25	2.78	2.89		2.88
80+80+80	3.45		3.11		2.44		2.50	
80+80+120			3.31				2.74	
90+90+50	3.67	3.56			3.33	3.40		
90+90+60	3.74	3.60	3.64		3.43	3.50	3.44	
90+90+120			4.44				3.37	
98+98+50	3.41	3.27			3.09	3.20		
98+98+60	3.55	3.38	3.30		3.19	3.31	3.22	
98+98+98	3.12	2.98	2.83	2.92	2.78	2.99	2.86	3.01
98+98+120			3.61				0.91	

Orbit Inclination Combinations
Column headings and row prefixes indicate inclinations included.

Table VII. Emitted Flux Flat Plate
Detailed Comparison of Some Polynomial Coefficients
Internal Consistency of System

Order Legendre Polynomial→	30°				40°				50°				60°			
Coefficient	0	1	2	3	0	1	2	3	0	1	2	3	0	1	2	3
80	255.78	4.20	-26.58	7.49	256.15	4.27	-26.95	6.09	256.30	5.61	-26.14	4.98	255.95	4.74	-25.98	5.76
	±4.74	±1.44	±0.61	±1.51	±3.86	±1.67	±0.29	±2.59	±3.65	±1.75	±1.61	±0.89	±4.22	±1.67	±1.59	±1.16
90	257.07	4.29	-26.57	6.65	257.48	4.60	-26.54	5.84	257.30	5.86	-26.66	4.57	257.02	5.10	-26.54	5.48
	±5.55	±0.52	±0.43	±0.87	±4.63	±1.61	±0.36	±1.90	±4.70	±1.36	±1.16	±1.10	±4.99	±1.52	±1.80	±0.86
98.6	256.82	3.91	-26.50	7.33	257.01	4.04	-27.07	5.90	257.08	5.52	-26.57	4.89	256.82	4.62	-26.39	5.61
	±5.66	±0.75	±0.70	±1.48	±4.64	±1.40	±0.29	±2.57	±4.37	±1.61	±1.88	±0.92	±4.98	±1.47	±1.82	±1.18
80+40	256.36	4.14	-27.06	7.28												
	±2.79	±1.57	±0.75	±1.88												
80+50	256.54	5.48	-26.28	6.94	256.70	5.23	-26.61	5.76								
	±2.37	±1.71	±0.48	±1.19	±2.24	±1.65	±0.75	±1.61								
80+60	256.32	4.63	-26.30	7.21	256.47	4.53	-26.62	5.96	256.50	5.43	-26.19	5.19				
	±2.71	±1.52	±0.37	±1.41	±2.51	±1.52	±0.57	±1.89	±2.57	±1.42	±0.97	±1.14				
90+40	257.35	4.11	-26.48	6.70												
	±3.32	±1.31	±0.70	±1.45												
90+50	257.13	5.11	-26.57	5.87	257.46	5.25	-26.57	5.30								
	±3.11	±1.20	±0.42	±0.99	±3.04	±1.39	±0.33	±1.39								
90+60	256.97	4.50	-26.56	6.51	257.27	4.78	-26.54	5.86	257.12	5.65	-26.62	4.99				
	±3.14	±1.37	±0.53	±0.85	±2.98	±1.58	±0.69	±1.39	±3.13	±1.35	±0.95	±0.84				
98+40	256.00	3.91	-26.93	7.14												
	±3.36	±1.34	±0.93	±1.83												
98+50	257.06	5.39	-26.39	6.91	257.19	5.15	-26.82	5.72								
	±2.84	±1.59	±0.47	±1.17	±2.70	±1.56	±0.81	±1.61								
98+60	256.90	4.50	-26.35	7.13	257.00	4.42	-26.77	5.85	257.03	5.36	-26.44	5.08				
	±3.31	±1.35	±0.37	±1.38	±2.98	±1.40	±0.57	±1.88	±3.04	±1.31	±1.04	±1.13				
98+98	256.78	3.99	-26.50	7.04	256.92	4.03	-26.96	5.76	256.97	5.16	-26.56	5.05	256.77	4.45	-26.45	5.50
	±3.76	±0.44	±0.23	±1.24	±3.43	±1.01	±0.76	±1.89	±3.39	±1.20	±1.53	±0.60	±3.75	±1.00	±1.48	±0.84
3L+18L	251.13	4.57	-26.22	7.10	251.77	4.60	-25.80	5.90	251.90	5.62	-24.37	5.07	251.28	4.95	-24.39	5.63
					only two sets availa[illegible], error estimate indeterminant											
10L+12L	262.42	3.40	-26.78	6.99	262.07	3.47	-28.12	5.61	262.04	4.70	-28.75	5.03	262.25	3.94	-28.50	5.37
					only two sets available, error estimate indeterminant											
	(257.25	4.79	-26.78	5.74	Reference Values) w/m^2 at satellite altitude.											

The error figure (±) is the standard deviation from the mean of the particular coefficient for all the different sets of equator crossings (Ω_o) within the system. (Reproducibility)

Note: normalized legendre polynomials were used.

Orbit combinations
Column heading plus row prefix indicate orbit inclination combinations.
3L, 18L, etc. indicate local time of sunsynchronous satellites.

Table VIII. Reflected Flux Flat Plate
Detailed Comparison of Some Polynomial Coefficients
Internal Consistency of System

Order Legendre Polynomial→ Coefficient ↓	30°				40°				50°				60°			
	0	1	2	3	0	1	2	3	0	1	2	3	0	1	2	3
80	111.30	53.33	5.01	11.09	112.93	54.86	5.25	10.46	113.29	54.25	4.89	11.20	112.91	54.68	5.23	9.36
	±13.77	±14.91	±9.02	±4.96	±8.25	±10.95	±8.73	±7.60	±5.94	±5.62	±3.91	±2.62	±8.46	±9.00	±5.11	±5.26
90	112.77	52.78	9.15	15.47	115.33	56.53	8.89	11.71	115.10	55.43	7.95	13.54	114.69	57.71	8.20	11.99
	±9.06	±15.08	±5.81	±7.61	±6.89	±7.53	±5.63	±2.60	±6.61	±5.71	±3.94	±3.08	±7.67	±8.05	±3.95	±2.08
98.6	115.74	97.40	9.50	-5.49	115.67	68.19	9.74	21.95	113.84	50.02	5.83	10.49	114.69	57.71	8.20	11.99
	±21.59	±49.17	±18.93	±20.28	±15.42	±31.01	±18.54	±22.23	±9.03	±8.66	±6.55	±7.46	±7.67	±8.05	±3.95	±2.08
80+40	113.14	55.01	5.07	10.71												
	±7.42	±10.55	±8.94	±7.06												
80+50	113.38	54.44	4.82	10.51	113.33	54.79	5.18	11.33								
	±4.73	±5.42	±4.46	±2.38	±4.38	±5.38	±4.37	±2.97								
80+60	113.28	55.04	5.11	9.85	113.45	55.38	5.48	10.41	113.38	54.99	5.19	10.27				
	±6.78	±8.70	±6.18	±5.11	±5.50	±7.72	±6.50	±5.65	±4.39	±5.60	±4.69	±4.74				
90+40	115.66	56.51	8.65	11.71												
	±6.29	±7.23	±5.78	±2.47												
90+50	115.27	55.90	7.86	12.70	115.06	56.08	8.03	12.64								
	±5.40	±5.43	±4.30	±2.69	±4.92	±5.04	±4.24	±2.77								
90+60	115.02	57.76	7.83	11.86	114.79	57.48	7.81	12.00	114.56	57.00	7.69	12.57				
	±6.45	±7.53	±4.50	±2.01	±4.89	±5.76	±4.34	±2.31	±4.54	±4.90	±3.51	±2.46				
98+40	116.12	68.40	9.23	22.28												
	±14.57	±29.98	±18.18	±21.16												
98+50	114.14	50.22	5.48	9.28	113.98	50.95	5.67	9.55								
	±7.90	±8.37	±6.89	±7.60	±7.50	±8.41	±6.63	±8.09								
98+60	113.08	52.18	6.70	7.60	113.36	52.56	6.99	7.75	113.25	52.25	6.92	8.10				
	±7.90	±11.24	±9.03	±8.30	±7.11	±10.68	±9.30	±9.11	±6.22	±8.21	±7.63	±7.56				
98+98	112.26	56.05	6.31	11.18	112.02	55.85	6.18	11.24	112.25	54.43	6.00	11.47	111.71	54.53	6.36	11.23
	±4.53	±5.07	±2.48	±2.94	±3.46	±3.99	±2.01	±2.77	±3.34	±2.48	±1.75	±1.44	±3.34	±2.87	±1.72	±2.51
3L+18L	120.69	65.21	10.13	14.23	118.04	62.30	8.82	14.24	117.24	57.33	5.40	11.05	116.41	59.24	6.96	12.14
					only two sets in system, variation indeterminant											
10L+12L	107.49	51.27	3.57	7.15	107.76	51.41	4.22	7.63	107.98	50.79	4.56	9.11	107.89	50.76	4.79	8.19
					only two sets in system, variation indeterminant											
	114.0	56.58	8.02	10.94	Reference Coefficients w/m^2 at satellite altitude.											

Orbit combinations
Column heading plus row prefix indicate orbit inclination combinations.
3L, 18L, etc. indicate local time of sunsynchronous satellites.

B. DISCUSSION, NON-SUNSYNCHRONOUS

The best system with two satellites is the 80^{o}, 50^{o} pair (Figs. 8 and 12). Using 8 and 29, errors of about $\pm$ 3.3 w/m^2 for emitted flux in the 7.5^{o} zone appear with worst case error much larger (Table III). These show good measurements within 50^{o} of the equator where there are two observing systems. Beyond there the single 80^{o} sensor shows poorer results.

Representing these results in terms of legendre polynomial coefficients, Table VII shows the global average result to be within 1.4% or 3.5 w/m^2 average error for the 80^{o} and 50^{o} combination. The higher order coefficients show similar amplitude errors resulting in higher precentage errors. The result for global average reflected flux is worse with a 5% or 6 w/m^2 error. Tables IV and V show application of Equation 29 to 10 coefficients.

The best three-satellite system is $80^{o}+60^{o}+50^{o}$ (Fig. 9). This is by no means an unambiguous decision as many of the different error measures give contradictory results. Another candidate for best three is $90^{o}+80^{o}+50^{o}$ (Fig. 10). The $80^{o}+50^{o}+60^{o}$ system has zonal average emitted flux errors of $\pm$ 2.6 w/m^2 and $\pm$ 5.3 in the reflected flux polynomial representation. The $90^{o}+80^{o}+50^{o}$ system is worse in the emitted error, ($\pm$ 2.8 w/m^2), but better ($\pm$ 2.6) in the reflected error. From the zonal average plots (Figures 10 and 11) $80^{o}+50^{o}+60^{o}$ was chosen as slightly better.

For reflected flux the results are poorer (Tables IV and VII) with large errors appearing even in the global average. This arises from the difficulty of measuring something with a large diurnal variation.

C. DISCUSSION, SUNSYNCHRONOUS WITH OTHERS

Two sunsynchronous satellites (98^{o}) and a 50^{o} (Fig. 12) give good error estimates. The zonal emitted flux errors are $\pm$ 2.7 w/m^2, $\pm$ 2.4 in the reflected and $\pm$ 1.3 appear in the emitted polynomial error estimates. As can be seen from Fig. 12 the worst errors can be very large. In Tables VI and VII two particular subsystems have been listed separately. The 3L and 18L refer to 3:00 local and 18:00 local equator crossings. Substantial systematic errors appear because of the fixed diurnal variations used in the simulation model. This will affect the accuracy of the system, but not the reproducibility. Essentially, measurements at one local time can measure changes from one period to the next if the change occurs throughout the day. It cannot measure the daily average radiation budget accurately unless the diurnal variation is known a priori.

The simulation model was not well designed for comparing sunsynchronous and non-sunsynchronous so we are reluctant to choose $98^{o}+98^{o}+50^{o}$ as a best three-satellite system, in view of systematic errors. More knowledge is needed about diurnal variations, especially systematic ones, for the analysis of any radiation budget measurements. This may become available with analysis of geosynchronous measurements.

VI. DECONVOLUTION

The measurement of the earth's radiation budget has been discussed here primarily in terms of measurements at satellite altitude. The task of climate and ocean-atmospheric modeling and climate monitoring would be simplified if the budgets were expressed in terms of fluxes at the top of the atmosphere, (50 km). Holloway (1957) first studied this problem using Explorer VII data and House did some studies with Tiros IV data.

A. Theoretical

A simple relation between the top of atmosphere radiation fluxes and measurements at satellite altitude comes about if some assumptions are satisfied. Essentially the two dimensional integral equation relating source to measurement can be inverted, provided that the average emission or reflection characteristic depends only on the relative positions of source flux and measurement sensor. The authors think that this assumption is adequately satisfied for the infrared flux in a time average. It is probably not adequate for the reflected flux as the strong bidirection reflectance characteristics are correlated with the variation in surface and atmospheric reflecting features. Perhaps in the zonal averages this problem can be overcome with some statistical reflection model. Experiments like ERB are needed to determine if this discussion is useful. This discussion is included as it is the only method available to convert radiation fluxes of one spherical surface around the earth to the radiation field on a surface of different radii.

The basic measurement equations, 1 and 2, can be recast in the form of equation 30.

$$m(\theta_s, \phi_s, t) = \int s(\theta,\phi,t)\, g(\theta_s,\phi_s,\theta,\phi,t)\, \frac{d\Omega}{\pi} \qquad (30)$$

The weighing function can be converted into two terms, h, depending on the relative location of (θ,ϕ), (θ_s,ϕ_s) and an anisotropic factor, ρ, which includes any dependence of g on absolute position (Eq. 31, 32).

$$m(\theta_s,\phi_s,t) = \int s(\theta,\phi,t)\, \rho(\theta,\phi,\theta,\phi,t)\, h(\gamma)\, \frac{d\Omega}{\pi} \qquad (31)$$

$$\cos\gamma = \cos\theta_s \cos\theta + \sin\theta_s \sin\theta \cos(\phi_s - \phi)$$
$$= \vec{r}_e \cdot \vec{r}_s \tag{32}$$

ρ = any dependence of g on absolute position

Clearly a time average is needed to obtain a reasonable measure m, Eq. 33.

$$\bar{m}(\theta_s,\phi_s) = \frac{\int m dt}{\int dt} = \int \frac{\int s\rho dt}{\int dt} h \frac{d\Omega}{\pi} = \int \overline{s\rho} h \frac{d\Omega}{\pi} \tag{33}$$

Now using the assumption that in the average the source flux is not correlated with the varying part of ρ, that is where ρ_o is a constant, varying probably near one, Eq. 34 and 35.

$$\int s\rho dt = \rho_o \int s dt \tag{34}$$

$$\bar{m}(\theta_s,\phi_s) = \int \bar{s}(\theta,\phi)\rho_o h(\gamma) \frac{d\Omega}{\pi} \tag{35}$$

This integral equation can be inverted easily since spherical harmonics are eigen functions of the operator $\int h(\gamma)\, d\Omega$. Expanding s, h and m in spherical harmonics (Eq. 36, 37, 38).

$$\bar{m}(\theta_s,\phi_s) = \sum_{n=o}^{n} \sum_{\ell=-n} m_n^{\ell} Y_n^{\ell}(\theta_s,\phi_s) \tag{36}$$

$$h(\gamma) = \sum_{i=o}^{\infty} h_i P_i(\cos\gamma) \tag{37}$$

$$\bar{s}(\theta,\phi) = \sum_{j=o}^{\infty} \sum_{k=j}^{j} s_j^k Y_j^k(\theta,\phi) \tag{38}$$

Where P's are Legendre polynomials and Y's are spherical harmonics.

The $\bar{m}(\theta_s,\phi_s)$ becomes

$$\bar{m}(\theta_s,\phi_s) = \sum_{j=o}^{\infty} \sum_{k=-j}^{j} \sum_{i=o}^{\infty} \int h_i \, s_j^k \, Y_j^k(\theta,\phi) \, P_i(\cos\gamma) \, \frac{d\Omega}{\pi} \tag{39}$$

Using the addition theorem for spherical harmonics, Eq. 40

$$P_i(\cos\gamma) = \frac{4\pi}{2i+1} \sum_{q=i}^{i} Y_i^q(\theta_s,\phi_s) \, Y_i^{q*}(\theta,\phi). \tag{40}$$

So the measurement becomes, Eq. 41

$$\bar{m}(\theta_s,\phi_s) = \sum_{j=o}^{\infty} \sum_{K=-j}^{j} \sum_{i=o}^{\infty} \sum_{q=-1}^{i} h_i S_j^K \, Y_i^q(\theta_s,\phi_s) \cdot \frac{4\pi}{2i+1} \int Y_j^k(\theta,\phi) Y_i^{q*}(\theta,\phi) \, \frac{d\Omega}{\pi} \, . \tag{41}$$

But the spherical harmonics are an orthonormal set so, Eq. 42

$$\begin{aligned} \bar{m}(\theta_s,\phi_s) &= \sum_{j=o}^{\infty} \sum_{K=-j}^{j} \sum_{i=o}^{\infty} \sum_{q=-i}^{i} h_i S_j^K Y_i^q(\theta_s,\phi_s) S_{ij} \delta_{Kq} \frac{4\pi}{\pi(2i+1)} \\ &= \sum_{j=o}^{\infty} \sum_{K=-j}^{j} h_j S_j^K Y_j^K(\theta,\phi) \, \frac{4}{(2j+1)} \, . \end{aligned} \tag{42}$$

Comparing the series expansion of $\bar{m}$ the corresponding coefficients can be found, Eq. 43.

$$\bar{m}_i^k = \frac{h_j S_j^k \, 4}{2j+1} = \lambda_j S_j^k \tag{43}$$

Thus a reasonably accurate measurement will determine the source function if h can be predicted. Table IX shows the eigen values, λ_j, for both spherical and plane sensors and assuming a diffuse radiation source.

Smith et al. (1975) discuss the propagation of errors associated with this inversion of the integral equation. Errors for calculating S_j^K multiply approximately as the reciprocal of λ_i^2. Effectively j is limited to less than ten with the measurement accuracies in m_i^K predicted. This is about the limit of the large coefficients in the data as discussed in section V above.

If the data are analyzed into regions rather than zones, 30 coefficients may be deconvoluted with error multiplication of less than five. The approximate ground resolution would then be 2000 by 2000 kilometers. The measurement coefficients, m_j^k, might have not been examined for k not zero. The errors in these calculations probably increase with bigger k, so the accuracies of regional fluxes would be less than for zonal averages.

B. Practical Considerations

After this discussion showing great promise, one must examine the assumption which makes it possible, namely that g depends only on the relative positions of the sensor and source points. For the pure geometrical factor this is not true because of non-circular orbits the non-circularity of the earth. But in the time average the pure geometry factor can be calculated exactly. As shown by Smith and Green (1975) an optimal estimate can be made of the S_j^k directly from the thousands of individual measurements, if h can be calculated for each measurement.

Predicting the variation of g caused by weather features and surface features is the real problem. Due to the absorption and emission of the

Table IX.

Eigen Values of Measurement Operator at 800 km.

Order	Plate	Sphere
0	.7894	1.082
1	.7804	1.067
2	.7628	1.036
3	.7374	.9923
4	.7055	.9374
5	.6682	.8740
6	.6272	.8051
7	.5840	.7335
8	.5399	.6619
9	.4963	.5926
10	.4542	.5274
11	.4143	.4676
12	.3771	.4138
13	.3430	.3662
14	.3119	.3246
15	.2836	.2885
16	.2580	.2571
17	.2346	.2297
18	.2134	.2055
19	.1939	.1839
20	.1760	.1644

atmosphere in the infrared, the so-called limb darkening, causes a decrease in the infrared radiance at large zenith angles. This is a 1 to 2% effect which depends only on the relative position to better than .1%. That is, the effects of changing weather on h can be predicted to better than .1%. Another anisotropic effect would be the shadowing in the infrared of the ground by clouds. This kind of effect is location dependent and is unpredictable. Experimental measurements must be made to determine the importance of this effect before the deconvolution technique can be applied. The ERB experiment and some experiments in GATE might provide some of these.

While deconvolution has good chance of being successful for the infrared emission, handling reflected measurements in this manner is much less certain. The large variation in the bidirectional reflectance and its dependence on surface type and sun position make g not independent of absolute position. In fact it will be impossible to predict the g for each individual measurement as there is no way to detect the distribution of surface and weather features in the field of view with integrating sensors. Requirements for concurrent high resolution data simply "begs the question". The best approach is to time and space average and to obtain some predictable statistical ensemble of reflection characteristics. For instance with a long enough time average, the cloud cover and surface features may approach a predictable mean state allowing an estimate of g and making it independent of absolute location.

Some of the conditions of h can be realized if one zonally averages the time average measurements before attempting an estimate of the source function.

$$M(\theta_s) = \frac{1}{2\pi}\iint m(\theta_s,\phi_s,t)dtd\phi_s$$
$$= \frac{1}{2\pi}\iint \frac{s(\theta,\phi)\rho(\theta,\phi,\theta_s,\phi_s,t)dt}{\int dt} h(\gamma)d\phi_s d\phi \frac{d\cos\theta}{\pi} \tag{44}$$

If ρ in the time average is dependent only on the relative longitudes $(\phi-\phi_s)$ then great simplification occurs. This is partly justified from the fact that the weather is largely zonally symmetric. A simplification occurs as both ϕ and ϕ_s extend all the way around the globe, Eq. 45.

$$M(\theta_s) = \int \frac{\int s(\theta,\phi)dt}{2\pi\int dt}\left[\int \bar{\rho}(\theta_s,\theta,\phi-\phi_s)h(r)d\phi_s\right]d\phi\frac{d\cos\phi}{\pi} \tag{45}$$

But $(\phi-\phi_s)$ takes on all values from 0 to 2π in the ρh integral so the bracket is independent of ϕ.

$$\bar{M}(\theta) = \int \bar{s}(\theta)\left[\int \bar{\rho}h(\gamma)d\phi_s\right]\frac{d\cos\theta'}{\pi} \tag{46}$$

The ρh integral can then depend only on θ and θ_s producing a one dimensional integral equation.

$$\bar{M}(\theta_s) = \int \bar{s}(\theta)\bar{\rho}(\theta,\theta_s)\frac{d\cos\theta'}{\pi} \tag{47}$$

Once again experimental measurements (e.g., from ERB on Nimbus 6) are needed to determine the accuracy of the assumptions on ρ to generate the one dimensional integral equation.

The deconvolution technique will also be useful to adjust real satellite measurements to one altitude above the earth. The satellites will probably be launched into slightly elliptical orbits with satellite-surface distances varying about 100 kilometers. This technique will allow adjustments of all measurements to a mean spherical surface. The smaller the adjustment distance the more accurate the method becomes. This in fact may be the most useful application of the deconvolution scheme.

Also, adjustments for different sensor geometries can be made. For instance, proposals have been made for medium resolution (10^{o} earth central angle) integrating sensors. These can then be combined with the full disc field of views of flat plates. Discussed below are spherical sensors compared to the flat plate.

C. Sample Tests

Applying these techniques to compare the fluxes with the measurements at satellite altitude (800 km) top-of-atmosphere by the reference set produce surprisingly good results. Expanding the zonal average of the source fluxes into Legendre polynomials, (Eq. 48), one can convolute the coefficients as in Equation 49. Then the predicted values of m and n produce Figure 13 and 14.

$$b_{io} = \int_{-1}^{1} \frac{\int s_{IR}(\theta,\phi)d\phi}{2\pi} P_i(\cos\theta)\,\frac{d\cos\theta}{\pi} \tag{48}$$

$$\begin{aligned} M_p(\theta_s) &= \text{predicted infrared flux} \\ &= \sum_i b_{io}\, P_i(\cos\theta_s)\lambda_i \end{aligned} \tag{49}$$

For the reflected the daily average incident flux must be multiplied by albedo (Eq. 50, 51, 52).

$$\bar{I}(\theta) = \int_{o}^{2\pi} I(\hat{r}_e \cdot \hat{r}_{sun})d_{sun}/2\pi \tag{50}$$

$$\bar{a}_{io} = \int\int \frac{a}{2\pi}(\theta,\phi)d\phi\; I(\theta)\; P_i(\cos\theta)\; d\cos\phi \tag{51}$$

and

$$\begin{aligned} N_p(\theta_s) &= \text{predicted reflected flux} \\ &= \sum_{i=o}^{a} \bar{a}_{io}\, P_i(\cos\theta_s) \end{aligned} \tag{52}$$

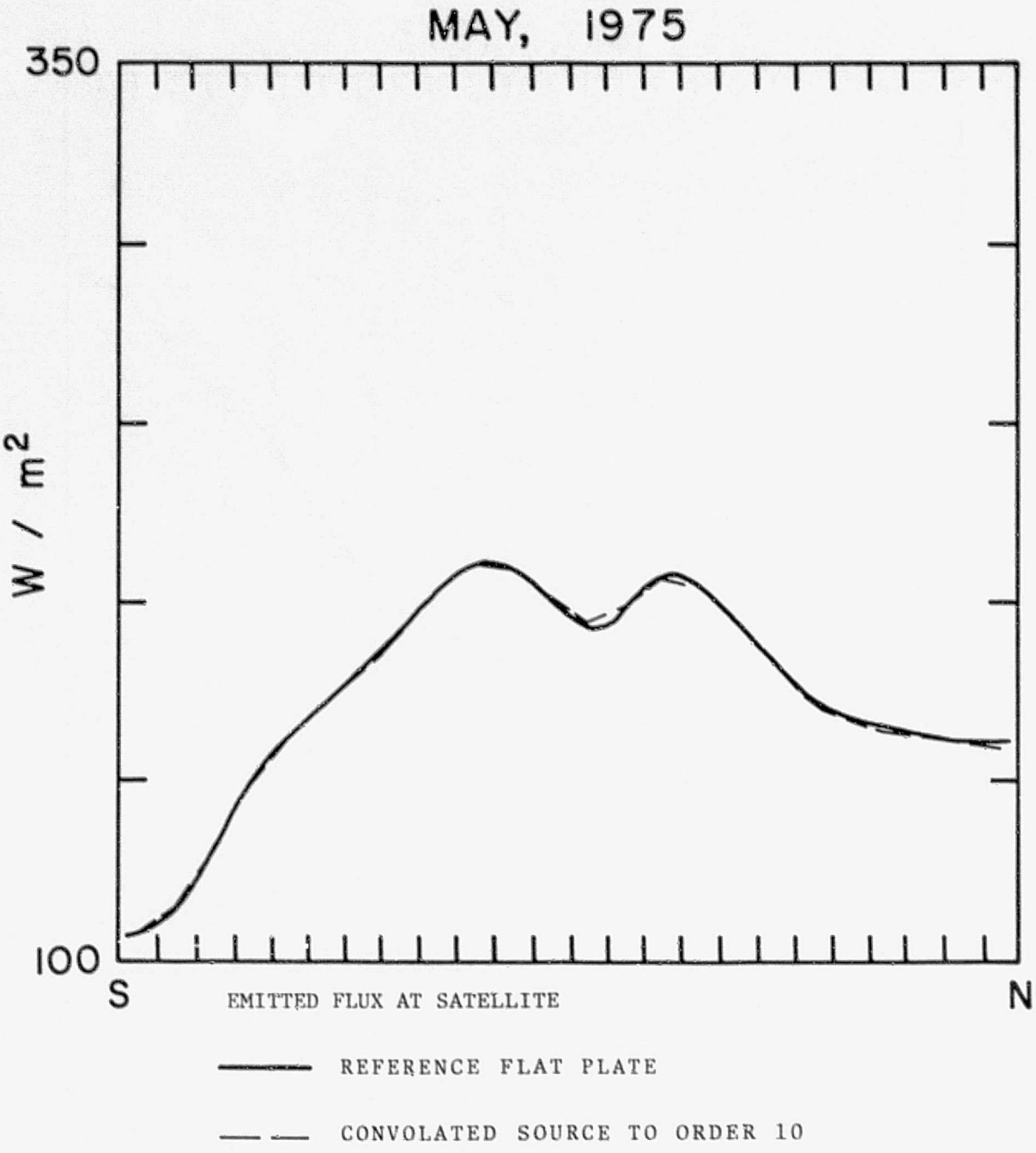
MAY, 1975
350
100
W / m²
S
N
EMITTED FLUX AT SATELLITE
REFERENCE FLAT PLATE
CONVOLATED SOURCE TO ORDER 10

FIG. 13

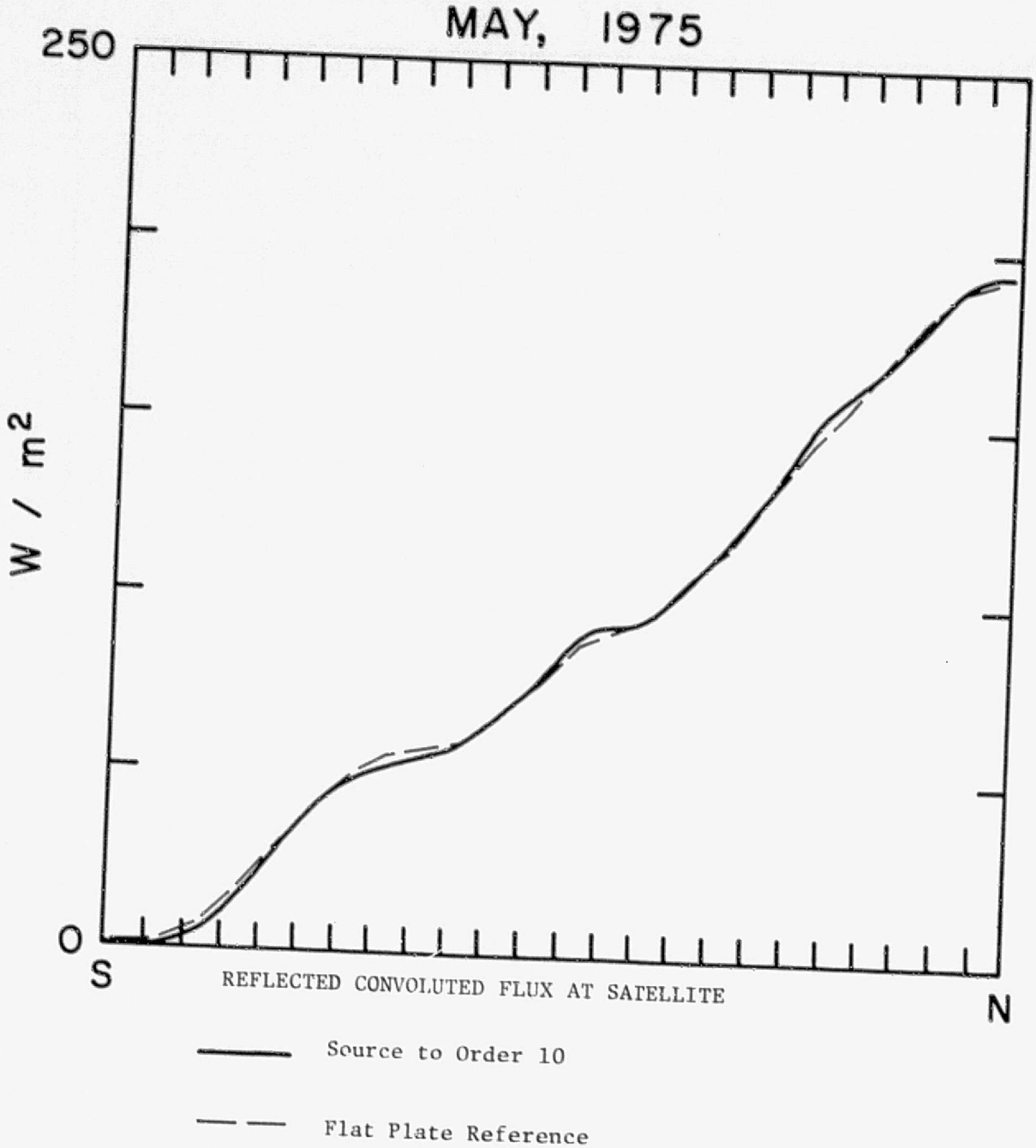

FIG. 14

Also shown in Figures 13 and 14 are the simple average of the ideal or reference measurement with its uniform space time sampling. The close agreement shows that the deconvolution procedure and its assumptions are not unreasonable.

The deconvolution of the reference set was also performed, Fig. 15 and 16, to predict the source function. The close correspondence, especially in the emitted term, is encouraging. The inaccuracy of utilizing orbital sampling with its imperfect space and time sampling degrades these results substantially. Figures 17 and 18 show deconvolutions of the best two satellite systems. The amplification of errors in the higher order terms is the cause of the wild oscillations especially in the reflected flux estimate.

VII. SPHERE VS. FLAT PLATE SENSORS

The results stated so far have been in terms of measurements by flat plate sensors which measure flux of radiation. A very similar integrating sensor, a sphere, can also be considered. The LZEEBE proposal included three 2 meter spheres. It has the great advantage that its orientation does not need to be controlled. Unfortunately, it does not measure energy flux.

One can calculate one measurement from the other if the source field has a unformly diffuse reflection or emission characteristic. Using this prediction method, Figures 19 and 20 show the reflected and emitted fluxes at satellite altitude estimated from the sphere measurement compared to the plate reference. The difference might be removed if one can predict more about the surface characteristics. But this can only be done with separate measurements or some statistical ensemble estimate of the characteristic. The difference between the measurements is a

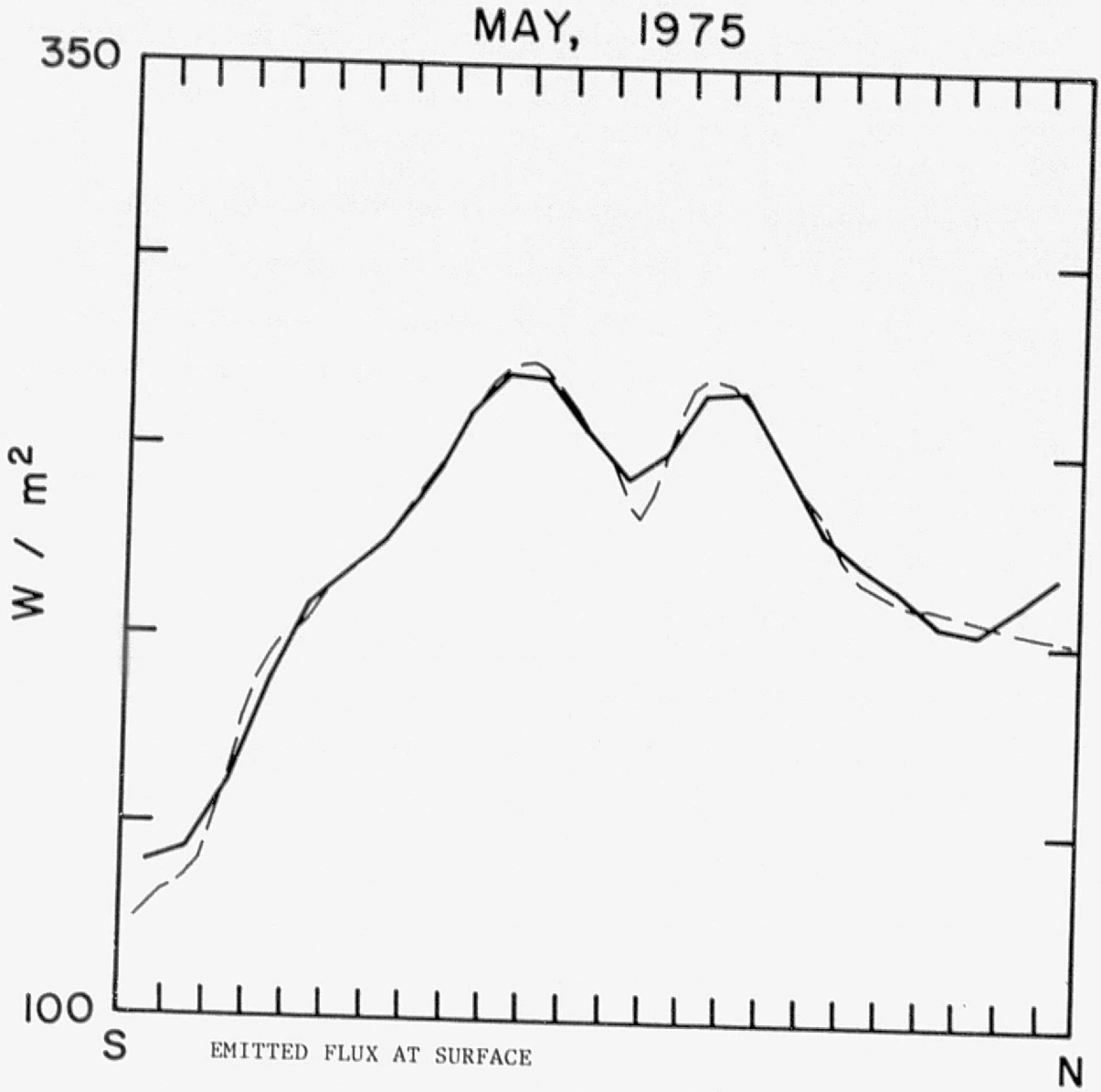

FIG. 15

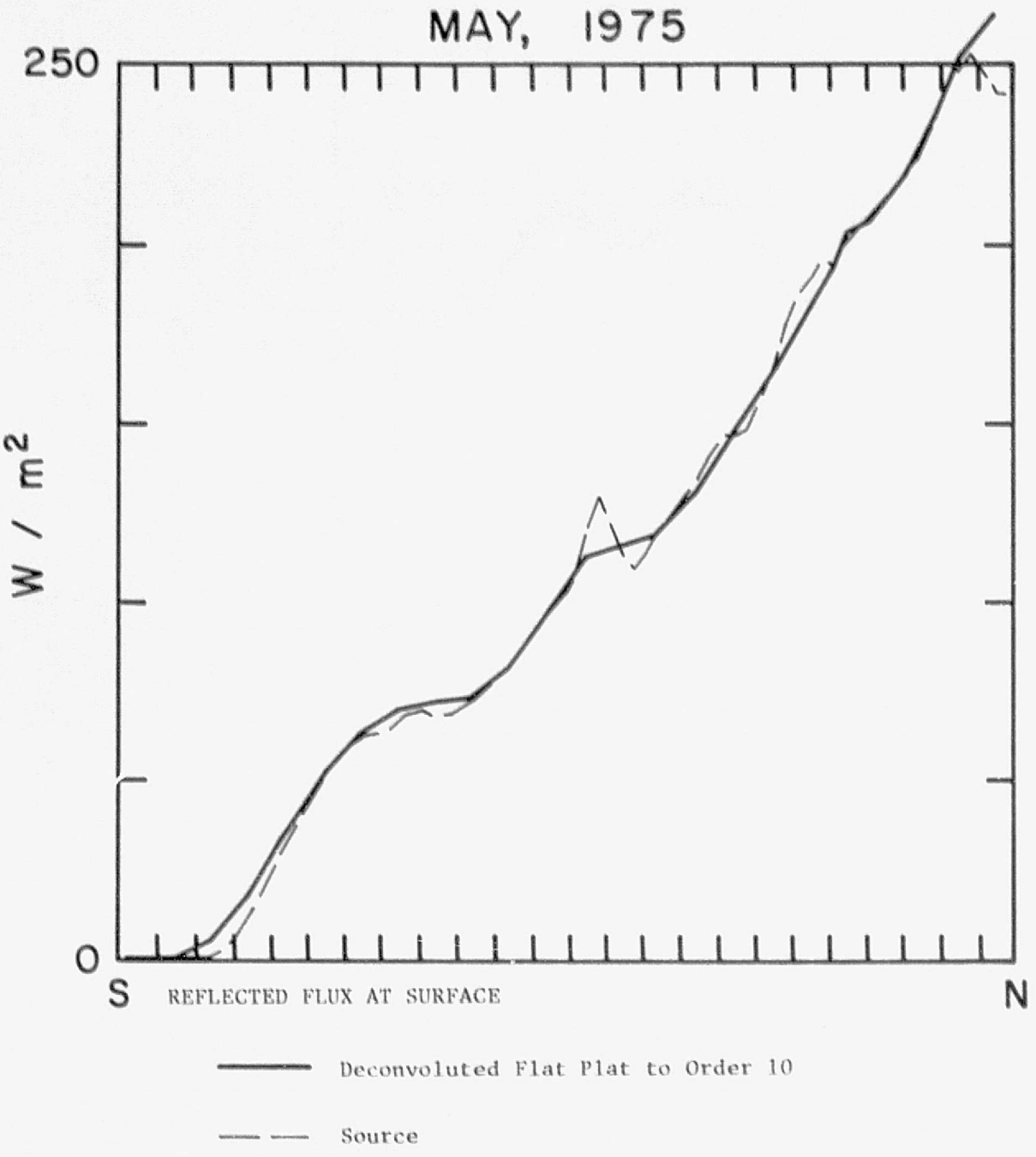
MAY, 1975
250
0
W / m²
S
REFLECTED FLUX AT SURFACE
N
Deconvoluted Flat Plat to Order 10
Source

FIG. 16

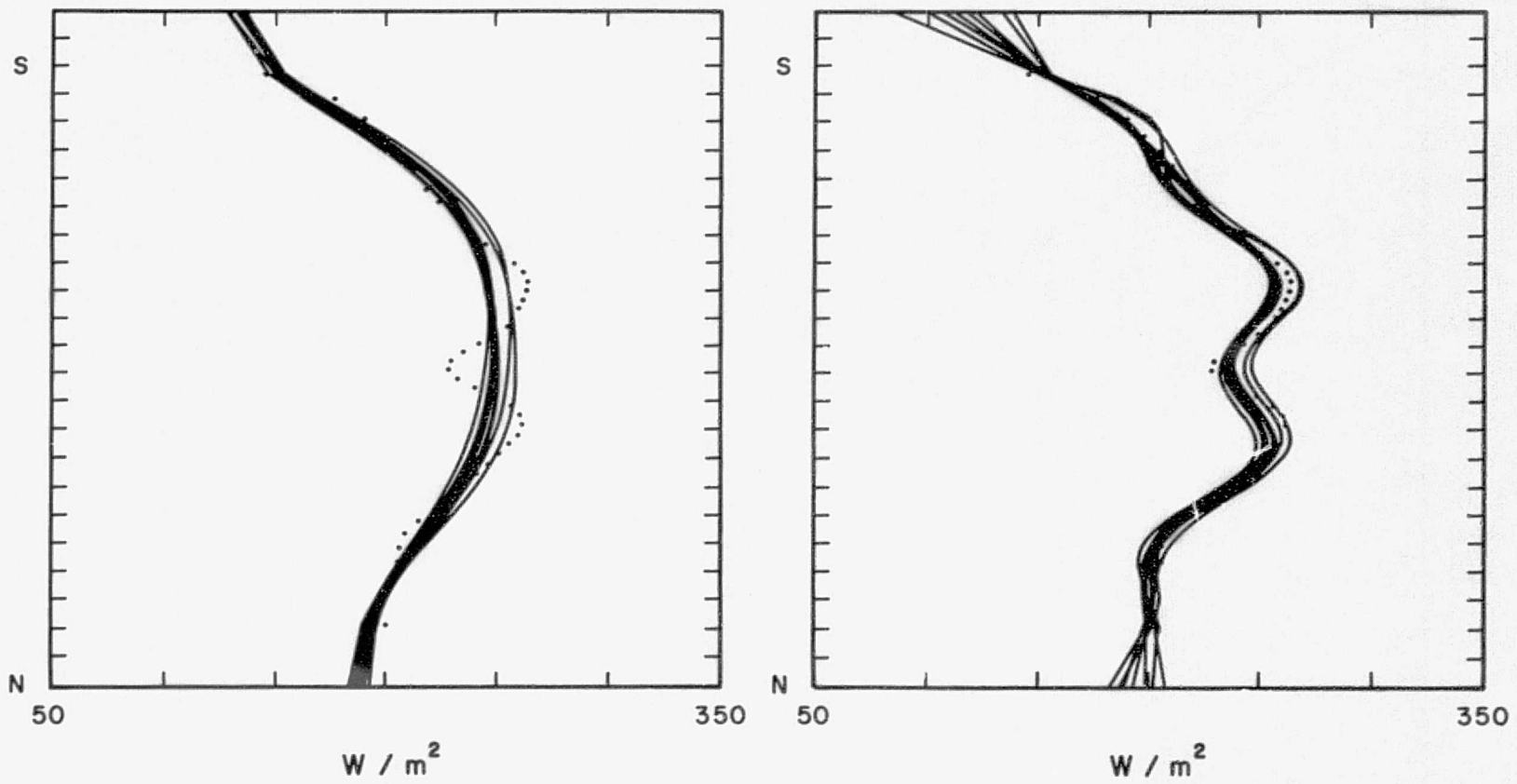

FIG. 17

REFLECTED FLUX AT SURFACE

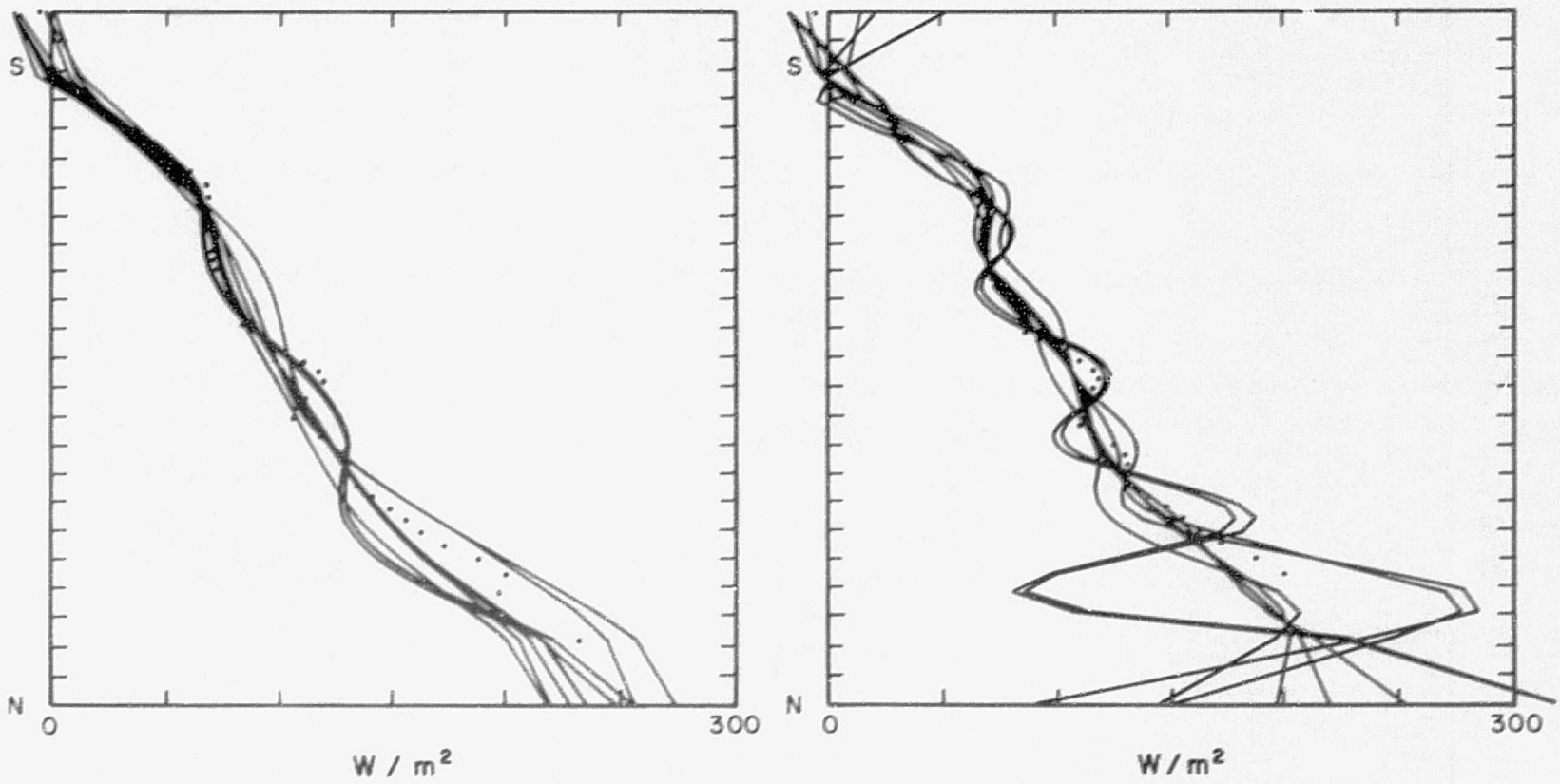

DECONVOLATION TO ORDER 6

DECONVOLATION TO ORDER 10

——— ESTIMATES FROM VARIOUS 50°+80° SETS

..... SURFACE SOURCE

FIG. 18

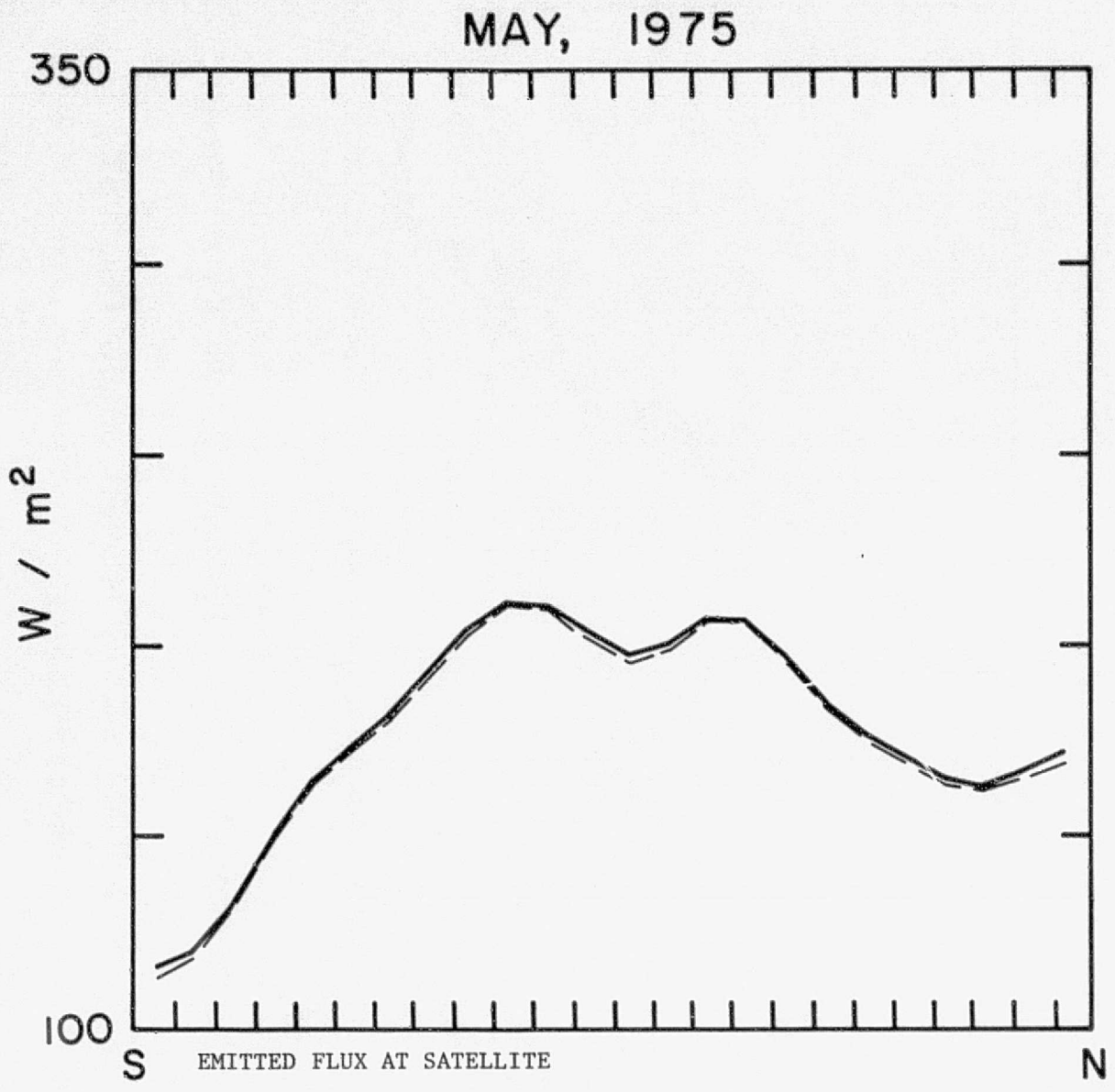

FIG. 19

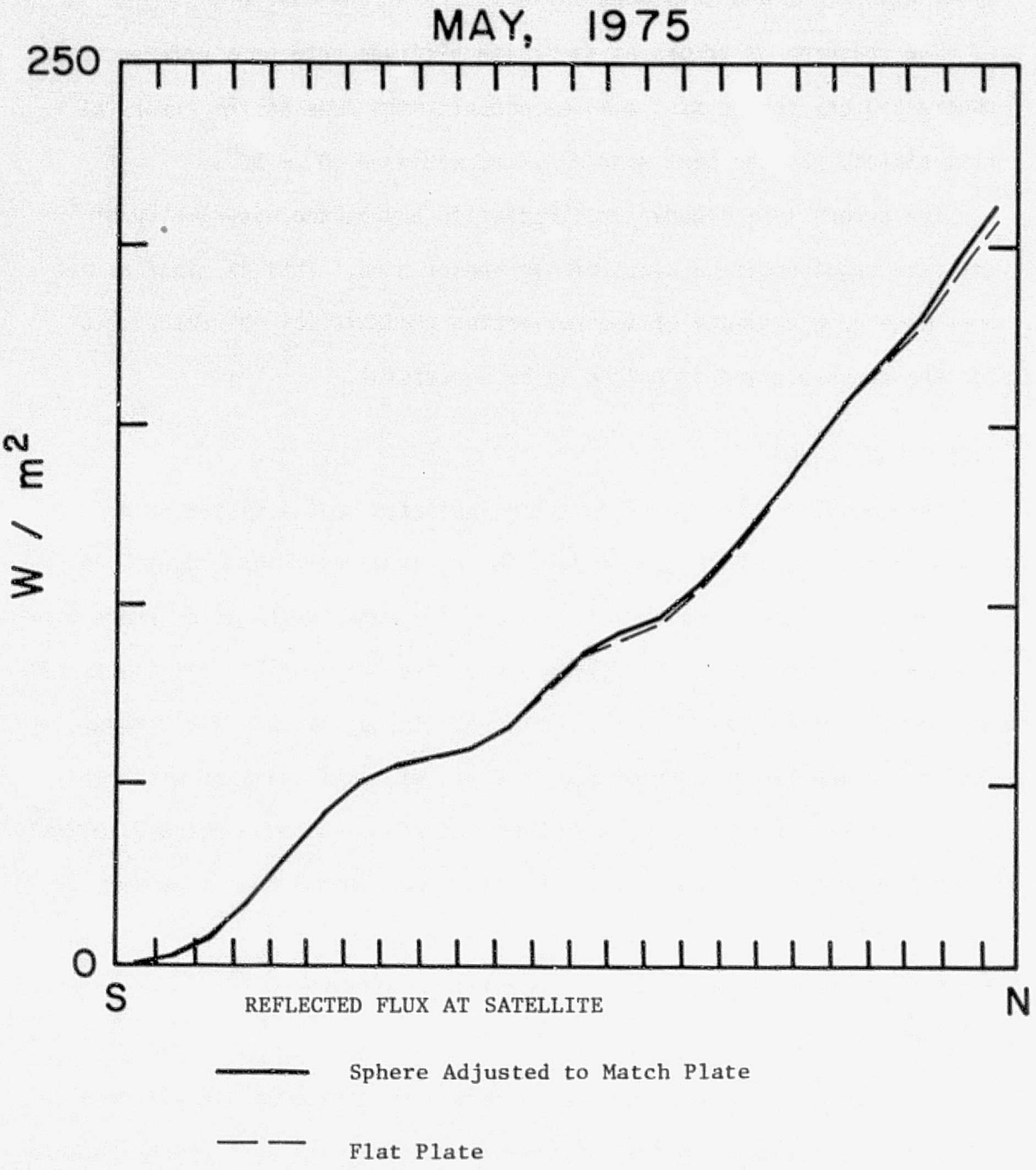
MAY, 1975
250
0
W / m²
S
N
REFLECTED FLUX AT SATELLITE
Sphere Adjusted to Match Plate
Flat Plate

FIG. 20

systematic error and thus more serious than a random error.

The measurement errors at satellite altitude between a reference sphere and any sphere system is essentially the same as the errors of flat plates. So the best sphere system would be 80^{o} + 50^{o}.

The errors in a deconvoluted radiation budget are essentially of the same magnitude regardless of the sensor used. This is clear as one must make good estimate of the reflection and emission characteristics for the deconvolution technique to be successful.

VIII. CONCLUSIO

The detailed numerical simulation indicates that a system of 80^{o} and 50^{o} inclined orbits can measure the earth's radiation budget with fair accuracy. In a measurement period of a month systematic errors of 1.5 W/m^2 will appear in the first 10 Legendre polynomial coefficients of emitted flux and 4. W/m^2 in the reflected flux at satellite altitude. The errors are larger when stated in terms of zonal averages with resolution of 7.5^{o} north-south, + 30 W/m^2 in reflected component and 10 W/m^2 in emitted worst, but average 6 W/m^2 and 3 W/m^2 zonal average errors. More satellites produce better results with errors of 1.3 W/m^2 emitted and 5.3 W/m^2 reflected for the polynomial [coefficients for a system of 80^{o}, 60^{o} and 50^{o})].

Sunsynchronous satellites plus others also give good overall results but larger worse case errors. Systematic differences will appear between different local time choices for the orbits because of the fixed diurnal variation used. This affects the accuracy of the daily average fluxes. The reproducibility of particular sets should be very good so changes could be measured well, sacrificing accuracy. One can conclude that if only one satellite is available any sunsynchronous orbit not near the

terminator is better than precessing orbits. It may not be accurate but at least it can measure changes unaffected by changes in sampling. More information about systematic diurnal radiation changes is critical for analysis combinations of synchronous and precessing orbits.

The deconvolution of the fluxes from satellite altitude to the top of the atmosphere requires very accurate measurements. With the estimated errors at most 10 polynomial coefficients can be deconvoluted giving a surface resolution of about 20^{o} N-S. The deconvolution technique will be useful though to normalize measurements to the same satellite altitude for systems with slightly elliptical orbits or different sensor geometries.

Finer resolution of orbit placement will require better simulation and analysis techniques. Some new experimental data will be needed on reflection characteristics to make this improvement.

To summarize fairly good accuracy can be obtained with precessing orbiting integrating sensors of the earth radiation budget. The most stringent criterion for obtaining high accuracy is the measurement of events at all local times.

ACKNOWLEDGEMENTS

We would like to than Jack Cooper, technical monitor, and the many other scientists at Langley Research Center of NASA for their ideas and support of this project. Also, the National Center for Atmospheric Research provided computer time for the simulation of the measurements.

REFERENCES

Holloway, L., 1957: Correcting for unavoidable smoothing of artificial satellite data. 155th Meeting of the American Meteorological Society, Washington, D.C., May 2.

House, F., 1975: Personal Communication.

Nimbus-6 User's Guide, 1975.

Raschke, E., T. H. Vonder Haar, M. Pasternak and W. R. Bandeen, 1973: The radiation balance of the earth-atmosphere system from Nimbus III radiation measurements. NASA Technical Note, D-7249.

Science Applications for Radiation Budget Measurements, NASA Workshop at NCAR(National Center for Atmospheric Research).

Smith, G. L., R. N. Green and G. G. Campbell, 1975: A statistical interpretation technique for wide angle radiometer measurements of earth energy budget. American Meteorological Society Fourth Conference on Probability and Statistics in Atmospheric Science. Tallahassee, Florida.

Smith, W. L., J. Hickey, H. B. Howell, H. Jacobowitz, D. T. Hilleary and A. J. Drummond, 1977: Nimbus-6 earth radiation budget experiment. Applied Optics, Vol. 16, p. 306.

Sikula, G. J. and T. H. Vonder Haar, 1972: Very short range local area weather forecasting from geosynchronous meteorological satellites. Atmospheric Science Paper #185, Department of Atmospheric Science, Colorado State University.

Vonder Haar, T. H., 1968: Variations of the earth's radiation budget. PhD Dissertation, Dept. of Meteorology, University of Wisconsin, Madison, Wisconsin.

Earth Radiation Budget Science Workshop, 1978: NASA Workshop at Williamsburg, VA, March, 1978 (in preparation).